

1 Intercomparison of Aerosol Optical Depths from four reanalyses and their 2 multi-reanalysis-consensus

3
4 Peng Xian¹, Jeffrey S. Reid¹, Melanie Ades², Angela Benedetti², Peter R. Colarco³, Arlindo da
5 Silva³, Tom F. Eck^{3,4}, Johannes Flemming², Edward J. Hyer¹, Zak Kipling², Samuel Rémy⁵,
6 Tsuyoshi Thomas Sekiyama⁶, Taichu Tanaka⁷, Keiya Yumimoto⁸ and Jianglong Zhang⁹

7
8 ¹Naval Research Laboratory, Monterey, CA, USA.

9 ²European Centre for Medium-Range Weather Forecasts, Reading, UK.

10 ³NASA Goddard Space Flight Center, Greenbelt, MD, USA.

11 ⁴University of Maryland Baltimore County, Baltimore, MD, USA

12 ⁵HYGEOS, Lille, France

13 ⁶Meteorological Research Institute, Japan Meteorological Agency, Tsukuba, Japan

14 ⁷Information Infrastructure Department, Japan Meteorological Agency, Tokyo, Japan

15 ⁸Research Institute for Applied Mechanics, Kyushu University, Kasuga, Japan

16 ⁹Department of Atmospheric Sciences, University of North Dakota, Grand Forks, ND

17
18 Corresponding author: Peng Xian (peng.xian@nrlmry.navy.mil)

19 20 21 Key Points:

- 22 1. Four global aerosol reanalyses are intercompared and verified with observations for their
23 skill in simulating aerosol optical depth.
- 24 2. The study identifies the strength of each reanalysis and the regions where there are
25 notable differences and challenges.
- 26 3. The multi-reanalysis-consensus, based on the four reanalyses, consistently ranks as one
27 of the best regionally and globally.

28 29 **Abstract**

30 The emergence of aerosol reanalyses in recent years has facilitated a comprehensive and
31 systematic evaluation of Aerosol Optical Depth (AOD) trends and attribution over multi-decadal
32 timescales. Notable multiyear aerosol reanalyses currently available include NAAPS-RA from the
33 U.S. Naval Research Laboratory; the NASA MERRA-2; JRAero from the Japan Meteorological
34 Agency (JMA); and CAMSRA from Copernicus/ECMWF. These aerosol reanalyses are based on
35 differing underlying meteorology models, representations of aerosol processes, and data
36 assimilation methods and treatment of AOD observations. This study presents the basic
37 verification characteristics of these four reanalyses versus both AERONET and MODIS retrievals
38 in monthly AOD properties and identifies the strength of each reanalysis and the regions where
39 divergence and challenges are prominent. Regions with high pollution and often mixed fine-coarse
40 mode aerosol environments such as South Asia, East Asia, Southeast Asia, and the Maritime

41 Continent pose significant challenges, as indicated by higher monthly AOD root mean square
42 error. Moreover, regions that are distant from major aerosol source areas, including the polar
43 regions and remote oceans, exhibit large relative differences in speciated AODs and fine-mode vs
44 coarse-mode AODs among the four reanalyses. To ensure consistency across the globe, a multi-
45 reanalysis-consensus (MRC, i.e. ensemble mean) approach was developed similar to the
46 International Cooperative for Aerosol Prediction Multi-Model Ensemble (ICAP-MME). Like the
47 ICAP-MME, while the MRC does not consistently rank first among the reanalyses for individual
48 regions, it performs well by ranking first or second globally in AOD correlation and RMSE,
49 making it a suitable candidate for climate studies that require robust and consistent assessments.

50

51 Keywords: Aerosol, Reanalysis, Aerosol Optical Depth, intercomparison, ICAP-MME

52

53 Short Summary

54 The study compares and evaluates monthly aerosol optical depth of four reanalyses (RA) and their
55 consensus (i.e. ensemble mean). The basic verification characteristics of these RA versus both
56 AERONET and MODIS retrievals are presented. The study discusses the strength of each RA and
57 identifies regions where divergence and challenges are prominent. The RA consensus usually
58 performs very well on a global scale in terms of how well it matches the observational data, making
59 it a good choice for various applications.

60

61 1. Introduction

62 In recent years, global aerosol reanalyses have been developed by major operational and research
63 centers, owing to the availability of long-record satellite remote sensing aerosol products and
64 advancements in aerosol data assimilation and modeling. These reanalyses are based on their
65 operational counterparts that are included in the "Core Four" members of the International
66 Cooperative for Aerosol Prediction Multi Model Ensemble (ICAP-MME C4C; Sessions et al.,
67 2015; Xian et al., 2019; Reid et al., 2022). The reanalyses include the Copernicus Atmosphere
68 Monitoring Service ReAnalysis (CAMSR; Inness et al., 2019) produced by the European Centre
69 for Medium-Range Weather Forecasts (ECMWF); the Japanese Reanalysis for Aerosol (JRAero)
70 (Yumimoto et al., 2017) developed by the Japan Meteorological Agency (JMA); the NASA
71 Modern-Era Retrospective Analysis for Research and Applications, version 2 (MERRA-2;
72 Randles et al., 2017); and the Navy Aerosol Analysis and Prediction System reanalysis (NAAPS-
73 RA; Lynch et al., 2016) developed by the U.S. Naval Research Laboratory (NRL).

74 The aerosol reanalyses are similar to their operational counterparts and characterized by a high
75 degree of independence in their underlying meteorology, aerosol sources, sinks, microphysics, and
76 chemistry, as well as in their assimilation methods for aerosol optical depth (AOD) observations.
77 A summary of the configurations of these four reanalyses is presented in Table 1 for general
78 features and Table 2 for microphysical and optical treatments of different aerosol species. Notably,
79 the use of operational Terra and Aqua Moderate Resolution Imaging Spectrometer data (MODIS
80 Dark Target and Deep Blue; Levy et al., 2013; Hsu et al., 2013) is consistent across these
81 reanalyses, although preprocessing treatments vary. These treatments include quality control, bias
82 correction, and aggregation and sampling. Additionally, several other products, such as
83 MultiAngle Imaging Spectroradiometer (MISR; Kahn et al., 2010), Advanced Very High
84 Resolution Radiometer (AVHRR; e.g., Ignatov et al., 2002), and Advanced Along-Track Scanning
85 Radiometer (AATSR, Popp et al., 2016) are assimilated into some of these reanalyses, although
86 these additional remote sensing data probably have only a small impact during the MODIS era, as
87 their data volume is small compared to MODIS. Therefore, between their underlying meteorology,
88 physics, and data assimilation these reanalyses are characterized by a high degree of independence
89 overall.

90 Like atmospheric reanalysis products, aerosol reanalysis products, whether used individually or in
91 combination, have been employed for diverse applications. They provide comprehensive aerosol
92 climatology and statistics to aid in understanding aerosol conditions across various regions and the
93 world (e.g., Reid et al., 2012; Xian et al., 2020; Nignombam et al., 2021; Ohno et al., 2022; Rubin
94 et al., 2023). They are widely used to address a multitude of scientific inquiries in the fields of
95 aerosol radiative forcing (e.g., Randles et al., 2017; Markowicz et al., 2017; 2021a,b; Ohno et al.,
96 2022; Zhang et al., 2023), aerosol-cloud interaction (e.g., McCoy et al., 2017; Ross et al., 2018;
97 Eck et al., 2018), aerosol-cryosphere interaction (e.g., Khan et al., 2018, 2019; 2020;
98 Roychoudhury et al., 2022), air quality and its impact on health (e.g., Tong et al., 2023; Cui et al.,
99 2022; Jenwithesuk et al., 2022; Lacima et al., 2022), biogeochemical cycles (e.g., Rahav et al.,
100 2020; Borchardt et al., 2019; Mescioglu et al., 2019), among others. These reanalyses have been
101 rigorously evaluated by the developing centers and various studies from different perspectives,
102 including AOD and other aerosol optical properties, mass concentrations, and vertical distribution
103 profiles. However, to date, no intercomparison among the four reanalyses has been conducted.

104 This study presents an intercomparison of the four available global aerosol reanalyses to evaluate
105 their skill in simulating monthly average AOD. Additionally, this study includes the development
106 of a Multi Reanalysis Consensus (MRC) product using a multi-model-consensus approach, similar
107 to the ICAP Multi Model Ensemble (ICAP-MME; Sessions et al., 2015; Xian et al., 2019). The
108 MRC is an ensemble mean (i.e., mathematical average) of the four individual reanalyses, with a
109 spatial resolution of $1^{\circ} \times 1^{\circ}$ latitude/longitude and monthly temporal resolution. The study provides
110 speciated AODs, fine-mode (FM), coarse-mode (CM) and total AODs at 550 nm for the period of
111 2003-2019 from three reanalyses, and all four reanalyses are available for the time period of 2011-
112 2019. In addition, a companion study focuses on global and regional AOD trends derived from
113 these reanalyses. The validation of AODs from the MRC, and the four component members, is
114 performed using ground-based AEROSol Robotic NETwork (AERONET; Holben et al., 1998)
115 observations, with MODIS AOD for spatial distribution evaluation. The validation results, as well
116 as the AOD climatology and divergence of the reanalyses, are presented in Section 3. The study
117 concludes with a summary of the findings in Section 4.

118

119 2. Data and Methods

120 This study intercompares the monthly average modal (total, FM, and CM) and speciated AOD
121 products from four aerosol reanalyses (RA) and their consensus, and evaluates the RA AODs with
122 AERONET and the combined MODIS Dark Target/Deep Blue retrievals (Levy et al., 2013; Hsu
123 et al., 2013).

124 2.1 Individual product lines

125 Descriptions of the four reanalysis datasets, including CAMSRA, JRAero, MERRA-2, and
126 NAAPS-RA v1, are provided in this section. Table 1 provides a summary of the basic features of
127 the four reanalyses and the MRC used in this study. Table 2 offers a summary of the parameters
128 employed to depict the microphysical and optical properties of aerosol species from these
129 reanalyses. Furthermore, Table 3 samples hygroscopic enhancement factor values that influence
130 optical property calculations due to the hygroscopic growth of particles at various relative humidity
131 levels. In addition to utilizing different meteorological data, aerosol source data, AOD
132 observations, and constructing aerosol species, notable differences exist even among similar
133 species regarding treatments related to aerosol microphysics, optical properties, and water uptake
134 ability for hydrophilic species.

135 2.1.1 CAMSRA

136 The Copernicus Atmosphere Monitoring Service (CAMS) Reanalysis (CAMSRA, Inness et al.,
137 2019) is run at the European Centre for Medium-Range Weather Forecasts (ECMWF) and is a
138 global reanalysis of atmospheric composition species, including aerosols. It builds on the
139 previous reanalyses of the MACC project (Inness et al., 2013) and the CAMS interim reanalysis
140 (Flemming et al., 2017). The CAMSRA is publicly available for the years 2003 to 2022 and is
141 being continuously updated for future years.

142 The CAMSRA is based on the Integrated Forecasting System (IFS) used by ECMWF for
143 numerical weather prediction and meteorological reanalysis. Two additional modules are
144 incorporated into the IFS for the CAMSRA, one to calculate the processes and reactions of the
145 chemical species and one to represent the prognostic aerosol species. The aerosol scheme
146 includes prescribed and online emissions, dry and wet deposition, production of sulfate from a
147 gas-phase sulfur dioxide precursor, and the aging of hydrophobic organic matter (OM) and black
148 carbon (BC) to hydrophilic. The prescribed anthropogenic emissions come from the MACCity
149 inventory (Granier et al., 2011) and the biomass burning (BB) emissions from the Global Fire
150 Assimilation System, version 1.2 (GFASv1.2) (Kaiser et al., 2012). GFASv1.2 is a separate
151 system to the IFS that uses satellite retrievals of fire radiative power to produce the BB emissions
152 that are then input as fixed emissions to the aerosol scheme. The transport of the aerosol species
153 by advection, convection and diffusion is calculated using the meteorological component of the
154 IFS and the wind fields from the meteorology are also used as parameters to estimate the online
155 sea salt (Monahan et al., 1986) and dust (Ginoux et al., 2001) surface emissions. One key
156 difference between the CAMSRA set up of the IFS and that used for numerical weather
157 prediction, is that for the CAMSRA the radiative impact of aerosol particles and ozone on
158 meteorology is also accounted for.

159 The observations used in the CAMSRA for aerosols are of total AOD at 550nm. These come
160 from MODIS collection 6 satellite retrievals for the entire period covered by CAMSRA and from
161 the Advanced Along-Track Scanning Radiometer for the period 2003-2012. These AOD
162 observations are simultaneously assimilated with trace gas and meteorological observations
163 using the 4D variational data assimilation system of the IFS with a 12-hour assimilation window.
164 The products available from the CAMSRA include speciated AODs at a 3-hour temporal and
165 approximately 0.7 degrees spatial resolution, whereas monthly mean AODs at 550nm were used
166 in this study.

167 2.1.2 JRAero

168 The Japanese Reanalysis for Aerosol (JRAero) was developed by the Meteorological Research
169 Institute (MRI) of the Japan Meteorological Agency and Kyushu University using the global
170 aerosol transport model MASINGAR Mk-2 (Yukimoto et al., 2012) and a two-dimensional
171 variational (2D-Var) data assimilation method. The model uses the MRI-AGCM3 atmospheric
172 general circulation model, and considers major tropospheric aerosol components, including black
173 carbon (BC), organic carbon (OC), mineral dust, sea salt, and sulfate aerosols, and their precursors.

174 JRAero assimilates global AOD from a bias-corrected MODIS Level 3 AOD product provided by
175 the US Naval Research Laboratory (NRL) and the University of North Dakota
176 (<http://doi.org/10.5067/MODIS/MCDAODHD.NRT.061>) every 6 hours. Anthropogenic and
177 biomass burning emissions were estimated using the MACCity (MACC/CityZEN EU projects)
178 emission inventory (http://accent.aero.jussieu.fr/MACC_metadata.php) and the Global Fire
179 Assimilation System (GFAS) dataset ([http://www.gmes-
atmosphere.eu/about/project_structure/input_data/d_fire](http://www.gmes-atmosphere.eu/about/project_structure/input_data/d_fire)). The reanalysis has a resolution of

181 TL159 (about $1.1^\circ \times 1.1^\circ$) with 48 vertical layers from the ground to 0.4 hPa. Validation results
182 and additional information can be found in Yumimoto et al. (2017).

183 2.1.3 MERRA-2

184 The NASA Modern-Era Retrospective Analysis for Research and Applications, version 2
185 (MERRA-2, Gelaro et al. 2017) is an atmospheric and aerosol reanalysis produced with the
186 NASA Goddard Earth Observing System (GEOS) Earth system model. Aerosol data assimilation
187 brings in data from the MODIS and MISR satellite sensors (after 2000) and includes AERONET
188 ground-based sun photometer observations (through 2014). The Goddard Chemistry, Aerosol,
189 Radiation, and Transport model (GOCART; Chin et al. 2000; Colarco et al. 2010) is run online
190 and radiatively coupled in the MERRA-2 system, and provides simulations of dust, sea salt,
191 sulfate, and black and organic carbon aerosol species.

192 Black and organic carbon are each partitioned into hydrophobic and hydrophilic modes, and a
193 single bulk sulfate aerosol species is carried. Dust and sea salt are partitioned into five non-
194 interacting size bins, with dust emissions based on the model 10-m wind speed and a topographic
195 source function following Ginoux et al. (2001), and sea salt emissions driven by the surface wind
196 friction speed modified from Gong (2003) and with a sea-surface temperature adjustment based
197 on Jaeglé et al. (2011). Explosive volcanic sulfur emissions are included through 2010 based on
198 Diehl et al. (2012), with a repeating annual cycle of degassing volcanic emissions subsequent.
199 Other emissions are as summarized in Table 1.

200 The analysis of AOD is performed on quality-controlled MODIS, MISR, and AERONET data as
201 described in Randles et al. (2017) and Buchard et al. (2015). The AOD analysis is performed by
202 means of analysis splitting, where first a 2-D analysis of AOD is performed using error
203 covariances derived from innovation data. Three-dimensional analysis increments for aerosol
204 mass concentration are then computed using the Local Displacement Ensemble (LDE)
205 methodology, which accommodates misplacement of the aerosol plumes due to source or
206 transport issues. The ensemble perturbations are generated at the full model resolution, without
207 the need for multiple model runs. Online quality control is performed as in Dee et al. (2001),
208 with observation and background errors estimated as in Dee and da Silva (1999). Randles et al.
209 (2017) and Buchard et al. (2017) describe the overall methodology and validation of the
210 MERRA-2 AOD reanalysis. For this study, monthly mean speciated AODs and total AOD at 550
211 nm with 0.5 degree latitude and 0.625 degree longitude spatial resolution were used.

212 2.1.4 NAAPS-RA v1

213 The Navy Aerosol Analysis and Prediction System (NAAPS, Lynch et al., 2016) is a global offline
214 chemical transport model developed at the U.S. Naval Research Laboratory. NAAPS simulates the
215 life cycles of aerosol particles and their gaseous precursors. The particle species include
216 anthropogenic and biogenic fine (ABF, a mix of sulfate, organic aerosols and BC from non-BB
217 sources), BB smoke, aeolian dust, and sea salt aerosols. The transport, hygroscopic growth of
218 particles, dry and wet removal processes of these particles, and emissions of wind-blown particles
219 are driven by the meteorological fields from the Navy Global Environmental model (NAVGEM,

220 Hogan, et al., 2014). Secondary organic aerosol (SOA) processes are represented with a 1st order
221 approximation method, in which production of SOA from its precursors is assumed to be instant
222 and is pre-treated outside the model. Anthropogenic emissions come from the MACC inventory
223 from ECMWF (Granier et al., 2011). BB smoke emission is derived from the Fire Locating and
224 Modeling of Burning Emissions (FLAMBE, Reid et al., 2009), which is constructed based on the
225 MODIS fire hot spot data. In the reanalysis version, additional orbital corrections and regional
226 emission factors are incorporated. Aeolian dust emissions are determined based on the surface
227 friction velocity to the fourth power, and surface erodibility, which is adopted from Ginoux et al.
228 (2001) with regional tuning. Dust emission occurs when specific conditions related to surface
229 wetness and friction velocity thresholds are met. The representation of sea spray process adheres
230 to Witek et al. (2007), with sea salt emission being governed by sea surface wind conditions.

231 The NAAPS-ReAnalysis (NAAPS-RA) v1 (Lynch et al., 2016) is derived from NAAPS, with
232 assimilation of quality-assured and quality-controlled MODIS (Zhang et al., 2006; Hyer et al.
233 2011) and MISR AOD products (Shi et al., 2011) using 2D-var data assimilation method (Zhang
234 et al., 2008). It provides 3-D mass concentration, extinction, and 2-D 550 nm AOD from these
235 aerosol species with 1°x1° latitude/longitude spatial and 6-hourly temporal resolution for the years
236 2003-2022. The BB smoke source and dust sources are regionally tuned to best match the FM and
237 CM AODs with AERONET AODs. Aerosol wet removals within the tropical region were
238 regulated with satellite precipitation product (Xian et al., 2009) to mitigate model's deficiency to
239 simulate convective precipitation. The reanalysis shows similar decadal trend of AOD found in
240 satellite products (e.g., Zhang et al., 2017) and was verified with various field campaign data (e.g.,
241 Reid et al., 2016; Atwood et al., 2017; Edwards et al., 2022; Reid et al., 2023) in addition to ground
242 and space-based observations.

243 2.2 Multi-reanalysis-consensus (MRC)

244 The MRC product is a result of combining four individual aerosol reanalysis products described
245 above. This method follows the multi-model-ensemble approach used by the International
246 Cooperative for Aerosol Prediction (ICAP) and is based on the work by Sessions et al. (2015) and
247 Xian et al. (2019). The data from each RA with spatial resolution different from 1°x1° lat/lon
248 degree, is first projected onto the global map with 1°x1° lat/lon degree resolution using linear
249 interpolation. Then the MRC value is determined by calculating the average of the values from the
250 four RAs. No weighting among the RAs is applied, or the four RAs are weighted equally in
251 deriving MRC. Regionally-weighted ensemble product based on the verification results shown
252 here can be developed in the future. The MRC provides speciated and total AOD at 550 nm with
253 a 1°x1° lat/lon degree and monthly resolution for the period 2003-2019. The MRC data for the
254 period spanning from 2003 to 2010 relies on three RAs, while for the period from 2011 to 2019, it
255 incorporates all four RAs, considering that JRAero data is only accessible starting from 2011.

256 Table 1. Summary of the characteristics of the aerosol reanalyses.

257

258

	Developer	Meteorology	Resolution lat x lon	DA method	Assimilated obs.	Species	Anthro. & Biogenic Emission	BB Emissions	Available time	reference
CAMSRA	ECMWF	Inline ERA5	0.7 x 0.7	4D-Var	DAQ MODIS, AATSR	BC, OM, Sulfate Dust, Sea Salt	MACCity (trend: ACCMIP +RCP8.5), monthly VOC	GFAS	2003-present	Inness et al., 2019
MERRA-2	NASA	Inline MERRA-2	0.5 x 0.6	2D-Var +LDE	Neural Net MODIS, MISR, AVHRR, AERONET	BC, OC, Sulfate Dust, Sea Salt	EDGAR V4.1, AeroCom Phase II	GFED before 2009, QFED after 2009	1980-present	Randles et al., 2017
NAAPS-RA	NRL	Offline NOGAPS/NAVGEN	1 x 1	2D-Var	DAQ MODIS, MISR	BB smoke, Dust, Sea Salt, ABF	MACCity, BOND POET, monthly SOA	FLAMBE	2003-present	Lynch et al., 2016
JRAero	JMA	Inline MRI AGCM3	1.1 x 1.1	2D-Var	DAQ MODIS	BC, OC, Sulfate Dust, Sea Salt	MACCity	GFAS	2011-present	Yumimoto et al., 2017
MRC	-	-	1 x 1	-	-	BB smoke, Dust, Sea Salt, ABF	-	-	2003-present	this work

259 Table 2. Parameters representing microphysical and optical properties of aerosol species from
260 the four aerosol reanalyses.

Species Models	Microphysics (sectional size bins in radius or bulk effective radius in μm)					Optical parameters at 550nm for the corresponding size bins (single scattering albedo, mass extinction efficiency m^2/g , and shape for dry particle)				
	Dust	Sea salt	sulfate/ABF	BB smoke /OC/OM	BC	Dust	Sea salt	sulfate/ABF	BB smoke /OC/OM	BC
CAMSRA	0.03 - 0.55, 0.55 - 0.9, 0.9 - 20	0.03- 0.5, 0.5 -5, 5 - 20	0.005 - 20	OM: 0.005 - 20	0.005 - 0.5	0.97; 2.56 0.90; 0.92 0.85; 0.42 sphere	1.0; 0.73 1.0; 0.14 1.0; 0.04 sphere	Sulfate 1.0; 4.33 sphere	OM: 0.89; 2.76 sphere	0.21; 9.41 sphere
MERRA-2	0.1 - 1.0, 1.0 - 1.8, 1.8 - 3.0, 3.0 - 6.0, 6.0 - 10	0.03 - 0.1, 0.1 - 0.5, 0.5 - 1.5, 1.5 - 5.0, 5.0 - 10	Bulk, 0.16	OC: Bulk 0.09	Bulk, 0.04	0.96; 2.02 0.92; 0.64 0.89; 0.33 0.83; 0.17 0.77; 0.08 spheroids	1.0; 0.73 1.0; 3.48 1.0; 0.74 1.0; 0.30 1.0; 0.10 sphere	Sulfate 1.0; 3.15 sphere	OC: 0.96; 2.67 sphere	0.21; 9.28 sphere
NAAPS-RAv1	Bulk, 2.5	Bulk, 1.5	Bulk, 0.14	Smoke: Bulk, 0.17	N/A	0.88; 0.59 sphere	0.99; 1.42 sphere	ABF 0.9; 3.48 sphere	Smoke: 0.89; 4.48 sphere	N/A
JRAero	0.100 – 0.159, 0.159 – 0.251, 0.251 – 0.398, 0.398 – 0.63, 0.63 – 1.00, 1.00 – 1.59, 1.59 – 2.51, 2.51 – 3.98, 3.98 – 6.30, 6.30 – 10.0	0.100 – 0.159, 0.159 – 0.251, 0.251 – 0.398, 0.398 – 0.63, 0.63 – 1.00, 1.00 – 1.59, 1.59 – 2.51, 2.51 – 3.98, 3.98 – 6.30, 6.30 – 10.0	Bulk, 0.15	OC: Bulk, 0.18	Bulk, 0.18	0.96; 1.78 0.98; 3.36 0.97; 3.32 0.94; 1.45 0.90; 0.82 0.86; 0.48 0.81; 0.29 0.75; 0.18 0.68; 0.11 0.61; 0.07 sphere	1.0; 0.17 1.0; 0.56 1.0; 1.36 1.0; 1.97 1.0; 1.53 1.0; 0.54 1.0; 0.39 1.0; 0.23 1.0; 0.14 1.0; 0.08 sphere	1.0; 2.26 sphere	0.96; 1.60 sphere	0.16; 5.34 sphere

261

262

263 Table 3. Hygroscopic enhancement factor (f) at different relative humidity (RH) levels for
264 various aerosol species in the four RAs. In MERRA-2, f for sea salt varies with size bins, thus a
265 range for f is presented here. Notably, NAAPS-RA v1 does not explicitly contain BC species.
266 More specific details can be found in the references provided in Table 1.

RH (%)	Sea salt				Sulfate/ABF				BB smoke/OM/OC				BC		
	CAMSRA	MERRA2	NAAPSRA	JRAero	CAMSRA	MERRA2	NAAPSRA	JRAero	CAMSRA	MERRA2	NAAPSRA	JRAero	CAMSRA	MERRA2	JRAero
<30	1.00	1.00	1.00	1.00	1.00	1.00	1.00	1.00	1.00	1.00	1.00	1.00	1.00	1.00	1.00
30	1.00	1.17-1.22	1.00	1.36	1.00	1.23	1.00	1.24	1.00	1.14	1.00	1.12	1.00	1.00	1.00
40	1.44	1.21-1.28	1.07	1.48	1.17	1.31	1.08	1.32	1.17	1.19	1.03	1.16	1.00	1.00	1.00
50	1.56	1.26-1.35	1.17	1.60	1.22	1.39	1.18	1.40	1.20	1.24	1.06	1.20	1.00	1.00	1.00
60	1.67	1.33-1.44	1.29	1.70	1.28	1.46	1.32	1.45	1.30	1.29	1.11	1.30	1.00	1.01	1.00
70	1.80	1.44-1.56	1.48	1.80	1.36	1.54	1.53	1.50	1.40	1.34	1.16	1.40	1.00	1.03	1.00
80	1.99	1.60-1.77	1.78	2.00	1.49	1.64	1.87	1.60	1.50	1.44	1.25	1.50	1.20	1.19	1.20
85	2.13	1.74-1.93	2.03	2.20	1.58	1.69	2.16	1.70	1.55	1.52	1.32	1.55	1.30	1.30	1.30
90	2.36	1.96-2.19	2.45	2.40	1.73	1.77	2.65	1.80	1.60	1.64	1.42	1.60	1.40	1.41	1.40
95	2.88	2.43-2.74	3.37	2.90	2.09	1.91	3.74	1.90	1.80	1.88	1.61	1.80	1.50	1.54	1.50

267

268 2.3 AERONET

269 AERONET is a global ground-based sun photometer network managed by NASA. Sun and sky
 270 radiance at multiple wavelengths, covering the near-ultraviolet to near-infrared, are measured
 271 (Holben et al., 1998). Version 3 Level 2 AERONET daily data (Giles et al., 2019), which are
 272 cloud-screened and quality-assured, are used in this study. The estimated uncertainty in
 273 AERONET measured AOD, due primarily to calibration uncertainty, is ~0.01-0.02 at optical
 274 airmass of one for network field instruments (with the highest errors in the UV; Eck et al., 1999).

275 The 550 nm FM and CM AODs and total AODs are derived with the Spectral Deconvolution
 276 Method (SDA; O'Neill et al. 2003). The AERONET SDA product has been verified using in situ
 277 measurements (see for example Kaku et al., 2014). The spectral separation of FM and CM particles
 278 is determined based on their distinctive optical properties and complete size distributions. As part
 279 of this separation, a diameter of approximately 1 μ m serves as an approximate threshold to
 280 differentiate FM and CM particles. This optical separation is different from the sub-micron fraction
 281 (SMF) method that uses a specified cutoff radius of the particle size distribution in the AERONET
 282 (AOD & sky radiance) inversion and allows more data to be available compared to the SMF
 283 method. The FM fraction based on SDA is generally comparable and slightly greater than SMF
 284 (O'Neill et al., 2023).

285 This study uses AERONET sites that have more than 5 years of observations and more than 1000
 286 daily data between 2011 and 2019 for verification purposes. Monthly AOD was derived for months
 287 that have more than 15 days of daily data. Then only sites with more than 45 total number of
 288 months (upper three quartiles of sites regarding total number of monthly data) were selected. This
 289 resulted in a total number of 200 sites globally. The list of sites along with latitude/longitude
 290 coordinates and elevation details for the studied regions is accessible in Table S1. Additionally,
 291 the locations of all sites can be identified in Figure 8.

292 2.4 MODIS AOD

293 Three MODIS AOD products are used as reference datasets to show global distribution of AOD
 294 climatology and the divergence among the retrieval products in comparison with the RAs. The
 295 level 3 MODIS AOD data for Dark Target (DT) were constructed using collection 6.1 Aqua
 296 MODIS level 2 DT data. The level 2 DT MODIS aerosol retrievals are available at a 10 \times 10 km²
 297 spatial resolution over both land and ocean. These aerosol retrievals were initially averaged on a

298 daily basis at a spatial resolution of $0.5 \times 0.5^\circ$ lat/lon. Only data with a quality flag of "marginal"
299 or better were used in the analysis. Additionally, retrievals with a cloud fraction larger than 80%
300 were excluded to minimize cloud contamination, as suggested by Zhang et al. (2005). The level 3
301 DT MODIS AOD data ($0.5 \times 0.5^\circ$ lat/lon) were then constructed using the daily averaged AOD
302 data.

303 Similar approaches were applied to C6.1 Aqua MODIS level 2 Deep Blue (DB) AOD data.
304 Unlike the MODIS DT aerosol retrievals, which are available over regions with low surface
305 reflectance, the DB retrievals are also available over some bright regions, such as desert regions.
306 No over-ocean aerosol retrievals, however, are included in the MODIS level 2 aerosol data. The
307 level 2 DB MODIS aerosol data were used to construct daily averages at a spatial resolution of
308 $0.5 \times 0.5^\circ$ (lat/lon). No quality flag and cloud fraction thresholds were applied. The level 3 DB
309 MODIS AOD data ($0.5 \times 0.5^\circ$ lat/lon) were constructed using the daily averaged AOD data.

310 The third MODIS AOD product is a data-assimilation-quality AOD dataset. It was based on C6.1
311 DT and DB retrieval products (Levy et al., 2013). Strict quality control and bias-correction
312 processes were applied as described in Zhang and Reid (2006) and Shi et al. (2011) for over water,
313 Hyer et al. (2011) for over land, and Shi et al. (2013) for over desert regions. These quality control
314 processes were updated for the C6.1 data and the final MODIS C6.1 AOD (550 nm) data is a level
315 3 product with $1^\circ \times 1^\circ$ lat/lon spatial and 6-hourly temporal resolution. This product has a cut-off at
316 40°S to filter out potential cloud-contaminated data south of this latitude. The 6-hour-averaged
317 AOD data were then binned into monthly means.

318 Note that MODIS AOD products are well known to low bias significant aerosol events (e.g., Reid
319 et al., 2022; Gumber et al., 2023) and slightly high bias clean environment (e.g. Wei et al., 2019),
320 which could affect AOD climatology to some degree.

321 2.5 Analysis Method

322 This study aims to investigate the divergence and utility of RAs for climate-scale studies by
323 exploring the AOD at 550 nm. To achieve this goal, the AOD data from the RAs, as well as
324 MODIS, were spatially and temporally binned into $1^\circ \times 1^\circ$ degrees and monthly resolutions. For the
325 purpose of verification and intercomparison analysis, only the data between 2011 and 2019 were
326 used as that is the period when all the RAs have data. The study focuses on the 550 nm AOD
327 parameter since it is available for all four aerosol RAs and MODIS. Furthermore, the AERONET
328 FM and CM AODs at 550 nm were obtained using the SDA method described in Sect. 2.3.

329 The study examines the performance of RAs globally and regionally. Sixteen regions, including
330 the globe, are defined for regional aerosol property analysis. They include East Asia, Southeast
331 Asia, South Asia, Maritime Continent, Australia, Southwest Asia, Europe, Northwest Africa,
332 South Africa, West North America, East North America, Central America, South America, as
333 indicated by the rectangular boxes in Figure 5, and Arctic (north of 70°N), and Antarctic (south of
334 75°S). There is no AERONET site satisfying site selection criteria as described in Section 2.3 in
335 the Arctic and Antarctic, so these two regions are excluded for regional verification though they
336 are included in other analyses.

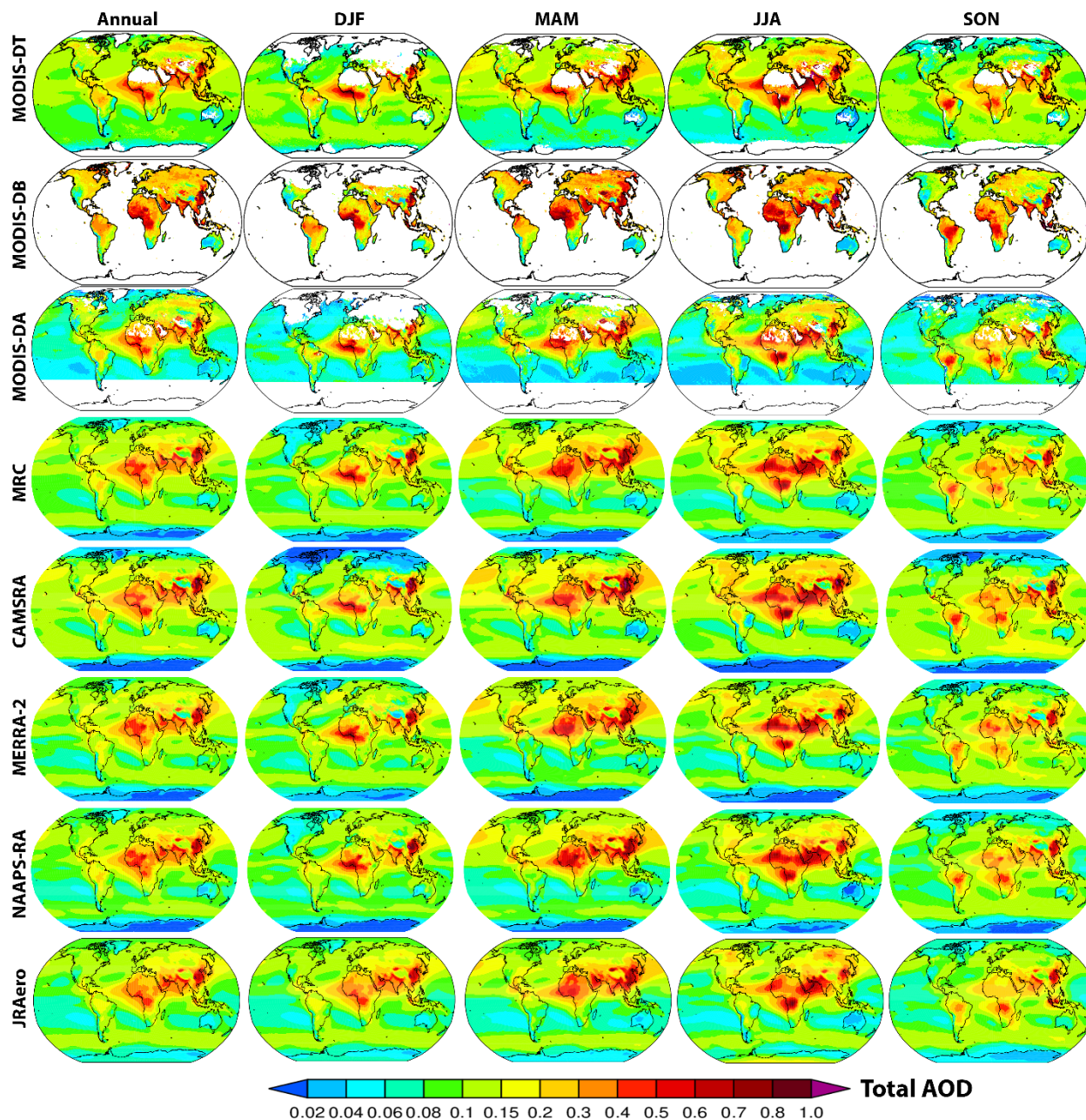
337 Regarding the aerosol species, the study focuses on BB smoke, ABF in NAAPS-RA, and its
338 equivalent of sulfate for MERRA-2, CAMSRA, and JRAero, as well as dust and sea salt. The
339 definition of species follows the ICAP practices (Sessions et al., 2015; Xian et al., 2019) for the
340 operational counterparts of these RAs and previous applications of these RAs (e.g., Xian et al.,
341 2022), in which the sum of OM and BC AODs from CAMSRA, and the sum of OC and BC AODs
342 from MERRA-2 and JRAero, is used to approximate BB smoke AODs. Although this separation
343 of species may be somewhat arbitrary, the study takes into account the fact that different aerosol
344 types and sources may be represented differently in each RA. For example, the NAAPS-RA model
345 characterizes aerosol species by emission source rather than chemical speciation, which makes it
346 unique. In contrast, CAMSRA, MERRA-2, and JRAero characterize OM or OC, BC, and inorganic
347 species, merging contributions from various anthropogenic, biomass burning and biogenic
348 sources.

349 The study also assumes that all sea salt and dust are CM, while other aerosol species are FM. The
350 segregation of sea salt and dust to the CM category is based on the fact that only a small portion
351 of total sea salt or dust AOD at 550nm are attributed to their FM components. For example, FM
352 sea salt represents about 17%, 10% and 11% of total sea salt AOD globally in MERRA-2,
353 CAMSRA and JRAero respectively. The numbers are about 30%, 39% and 32% for dust. While
354 FM fraction of dust during dust storms in Africa varies between 20-25% according to AERONET.
355 The FM fraction of dust from MERRA-2, CAMSRA and JRAero might be biased high as these
356 global models tend to overestimate FM dust and underestimate CM dust (for example O'Sullivan
357 et al., 2020; Kramer et al., 2020). In contrast, NAAPS-RA assumes all sea salt and dust are CM.
358 Verification results based on the FM and CM AODs derived using the FM fractions of sea salt and
359 dust from MERRA-2, CAMSRA and JRAero can be found in the supplemental material (Fig. S2-
360 4). Generally, the validation of FM and CM AODs with AERONET data shows a degradation in
361 performance for the three RAs compared to the verification results presented below, as discussed
362 in section 3.3.1.

363 For every AERONET site, the time series of monthly modal AOD from each RA is first extracted
364 from the model grid that encompasses the site's location. Bias, root mean square error (RMSE),
365 and coefficient of determination (r^2) are then computed for each site and each RA. The regional
366 validation outcome is derived from the average of validation statistics across all sites within the
367 region (see Table S1 for the sites included in each region). Following the criteria for site selection
368 outlined in section 2.3, only 200 sites are available globally, and certain regions have only a few
369 sites (a minimum of three sites, such as in South Africa) to represent the entire region; hence, no
370 site weighting within a region is applied. It is acknowledged that this averaging method could bias
371 the global validation result toward regions densely populated with sites, notably North America
372 and Europe. The AOD validation results for total, FM, and CM AOD at 550nm are presented
373 accordingly.

374 3. Results

375 3.1 Total and speciated AOD climatology



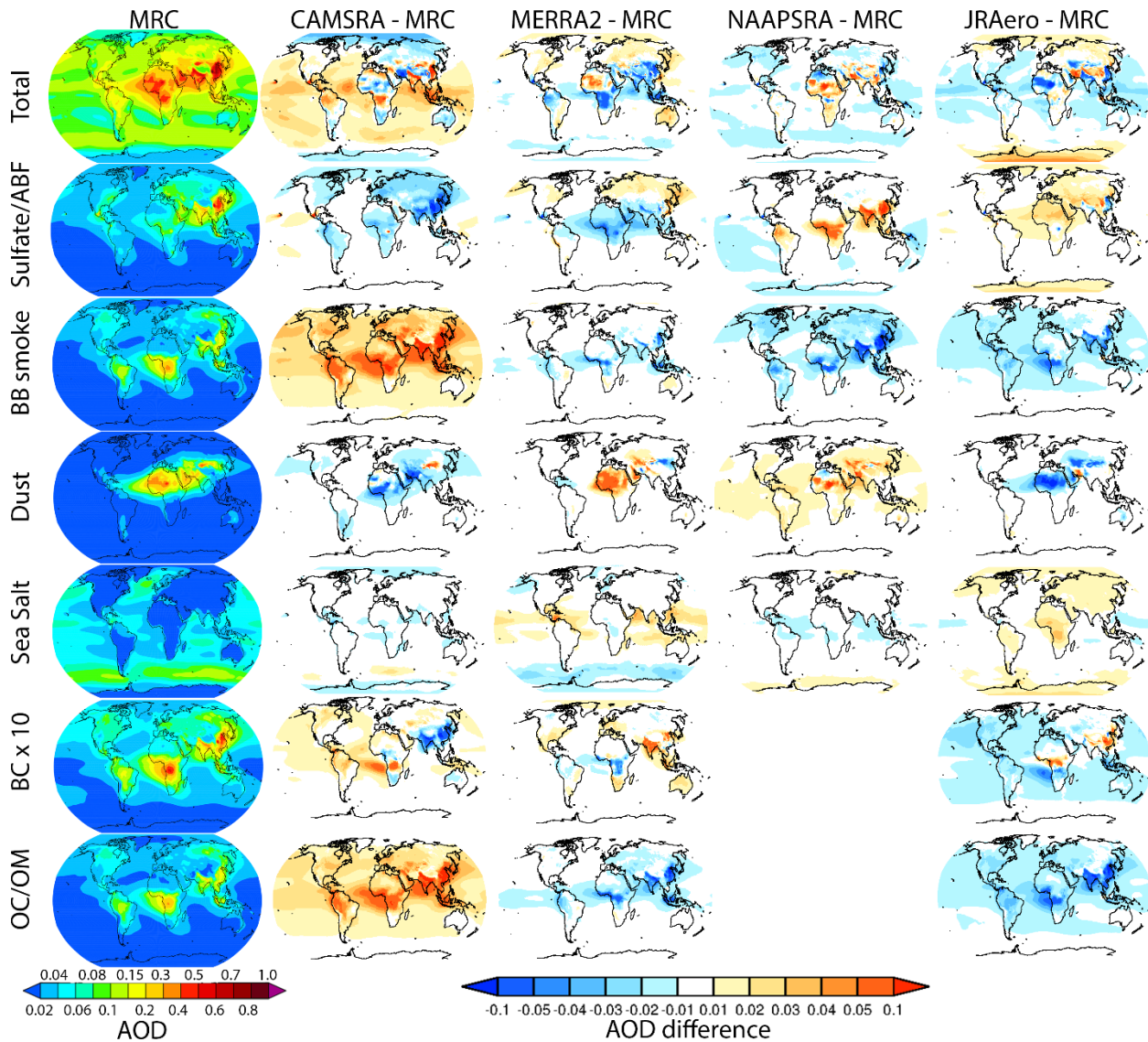
376

377 Figure 1. Annual and seasonal total 550nm AOD climatology from three MODIS products, the
 378 four RAs, and the MRC over 2003-2019, except JRAero for 2011-2019. MODIS-DA is the data-
 379 assimilation-quality AOD dataset described in Section 2.4. In the MODIS plots, the white area
 380 means a lack of data attributed to either none valid-retrievals or quality-control filtering.
 381 Notably, MODIS-DB data is only available over land.

382 The climatological annual and seasonal mean total AODs at 550nm from the three MODIS AOD
 383 datasets and the four aerosol RAs and the MRC are presented in Figure 1. In general, there are
 384 very similar spatial AOD distribution patterns and AOD magnitude among the RAs and MODIS

385 datasets for all four seasons. This is expected as MODIS total AOD is assimilated into all of these
386 RA products as well as used to tune the model components such as emissions. High AOD regions
387 include the dust-dominated Sahara in Mar-Apr-May (MAM) and Jun-Jul-Aug (JJA), Sahel in Dec-
388 Jan-Feb (DJF) and MAM, Southwest Asia and Taklamakan in MAM and JJA, anthropogenic
389 pollution-dominated East Asia and South Asia throughout the year, BB smoke-dominated South
390 Africa, South America in JJA and Sep-Oct-Nov (SON), Southeast Asia in MAM, Maritime
391 Continent in SON, and high-latitude North America and Eurasia in JJA. For the annual mean,
392 MODIS AODs from all the three products are relatively high compared to the MRC in the northern
393 hemisphere's high latitudes due to seasonal sampling bias. MODIS was able to retrieve AOD
394 during biomass burning active season, i.e. boreal Summer-to-Fall, but it couldn't retrieve AOD
395 during northern winter in the high latitudes due to the lack of sunlight and the high snow/ice
396 coverage. The high AOD over high-latitude Eurasia and North America in MODIS annual mean
397 is a general reflection of MODIS summertime AOD, which is captured by all the RAs in their
398 summertime mean AODs.

399 It is worth noting that MODIS-DB AOD generally exhibits slightly higher values compared to
400 MODIS-DT AOD, except in high terrain regions (e.g., Western North America). On the other
401 hand, MODIS-DA AOD tends to be slightly lower (approximately 0.02 magnitude) than MODIS-
402 DT AOD over oceanic regions due to bias-correction procedures. When compared to MODIS-DT,
403 AODs from the RAs tend to align more closely, especially over oceanic areas. Furthermore, RAs
404 typically exhibit lower AODs compared to MODIS-DB over regions affected by African and
405 Arabian dust. Overall, the divergence in total AOD climatology among the RAs is comparable to
406 or even smaller than the divergence observed in the MODIS products.



407

408 Figure 2. Annual mean total and speciated AODs of the MRC and the AOD difference between
 409 the individual RA and the MRC based on the 2011-2019 average. BB smoke is approximated as
 410 the sum of OC/OM and BC in CAMSRA, MERRA-2 and JRAero.

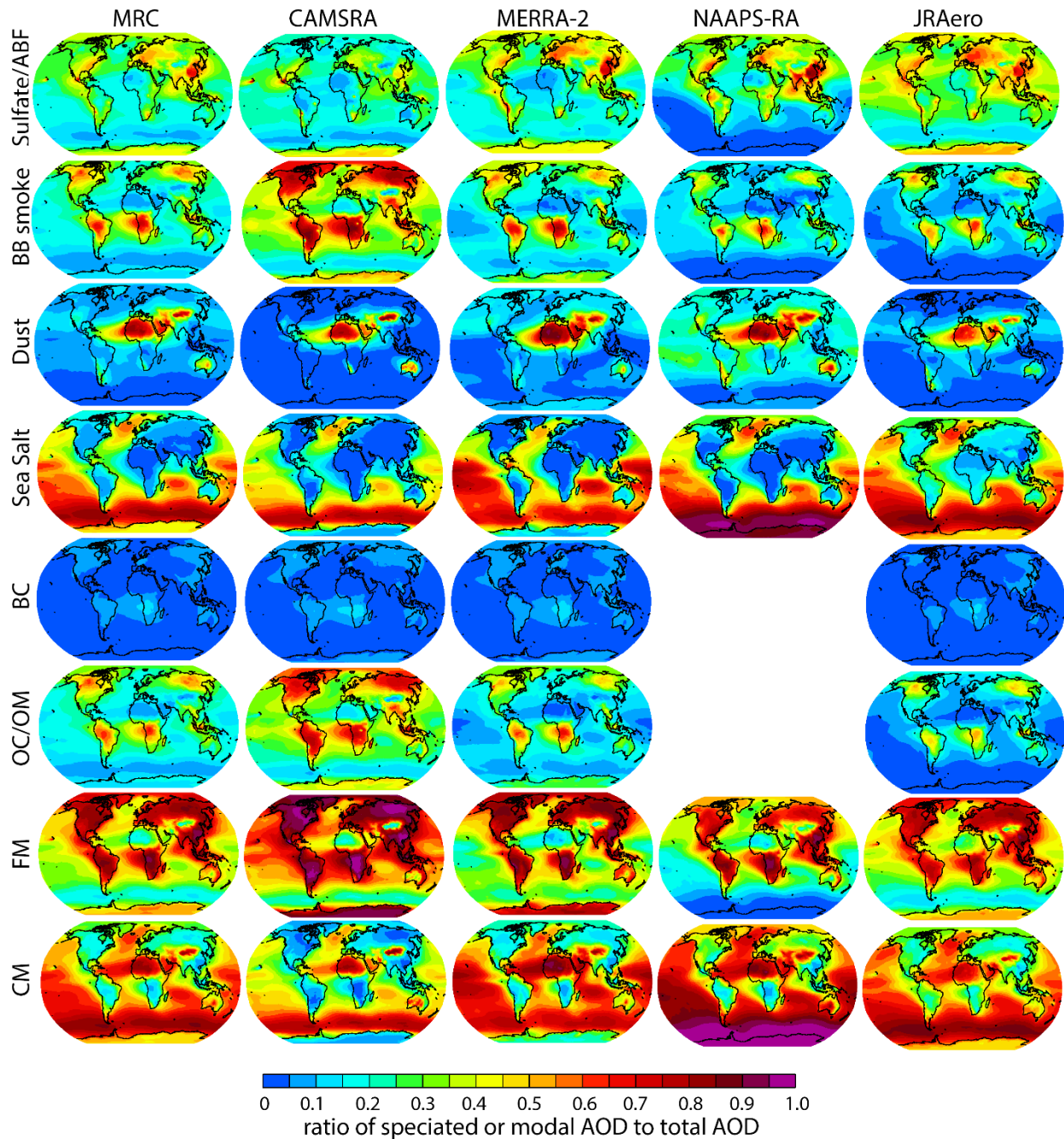
411 Previous experience with multi-model ensembles suggests that the consensus of multi-models, in
 412 general, shows better skill than individual contributing models (Sessions et al., 2015; Xian et al.,
 413 2019; Reid et al., 2022). Similar verification conclusion is also drawn in Section 3.3. Therefore,
 414 the total and speciated AODs from the MRC based on the 2011-2019 average are used as a baseline
 415 here and are shown in Figure 2. As expected, sulfate/ABF AOD is relatively high over population-
 416 dense and industrially polluted regions, dust AOD is high over major desert and arid regions, and
 417 sea salt AOD is relatively high over mid-to-high latitude oceans. BB smoke and its components
 418 BC and OC/OM are relatively high over South Africa, South America, Southeast Asia, the
 419 Maritime continent, and Siberia, North American high latitudes major BB source regions. BC and
 420 OC/OM AOD are also relatively high over South Asia and East Asia, where sources other than

421 BB, such as anthropogenic emission, are the main contributors, as suggested by contrasting smoke
422 AOD contribution to the total AOD between NAAPS-RA and other RAs in these regions (Figs 3
423 and 10. Noting that smoke AOD is driven by BB in NAAPS-RA, while smoke AOD is a sum of
424 BC and OC/OM from the other RAs).

425 Shown also in Figure 2 are the total and speciated AOD differences between the individual RA
426 and the MRC. For total AOD, CAMSRA is apparently higher than the other three RAs over the
427 ocean, which is consistent with the findings on its operational counterpart of high biased FM AOD
428 verified with Maritime Aerosol Network over the ocean in Reid et al. (2022). This high bias is
429 attributed to its universally higher OM/smoke AOD compared to other RAs, and suggests that
430 CAMSRA may have higher BB emissions and/or higher secondary production of OM compared
431 to the other RAs. Sulfate AOD is relatively low in CAMSRA except for some highly biased
432 hotspots around outgassing volcanoes (in particular Mauna Loa and near Mexico City) as
433 mentioned in Inness et al (2019). Differences in species definitions affect the comparison with
434 NAAPS-RA: NAAPS-RA ABF AOD is higher than sulfate AOD in other RAs especially in East
435 Asia, South Asia, central Africa, and north South America, and these deviations are
436 counterbalanced by opposite deviations in the BB AOD. This is expected as ABF in NAAPS-RA
437 includes additional aerosol sources besides sulfate, and some of these sources are included in the
438 BB AOD for other models. For dust AOD, MERRA-2 is relatively higher over north Africa and
439 the Arabian Peninsula and NAAPS-RA is relatively higher over most regions, including oceanic
440 areas, while CAMSRA and JRAero are relatively lower over most regions except around Gobi
441 desert for CAMSRA and Iran for JRAero. As for sea salt AOD, MERRA-2 is relatively higher
442 over the tropical oceans, and lower over the southern ocean. JRAero sea salt AOD is relatively
443 higher over most continents, which is probably unphysical.

444 The differences in speciated AOD result in significant variations in their contributions to the total
445 AOD, as illustrated in Figure 3. For instance, the considerably higher BB smoke AOD in
446 CAMSRA compared to other RAs makes BB smoke the predominant contributor to total AOD in
447 the CAMSRA over most continents, adjacent water bodies, and polar regions, except for regions
448 where dust is dominant. Sulfate AOD, on the other hand, contributes more to the total AOD,
449 particularly over oceanic regions in the JRAero compared to other RAs. Both MERRA-2 and
450 JRAero exhibit higher sulfate contributions along the western coasts of South America and North
451 America, suggesting possible increased production of dimethyl sulfide (DMS) in those areas. Dust
452 AOD, on the other hand, contributes more to the total AOD particularly over oceanic regions in
453 NAAPS-RA compared to the other RAs. Sea salt AOD is found to contribute more to the total
454 AOD in the high-latitude oceans and the Antarctic in NAAPS-RA compared to the other RAs. The
455 OC/OM AOD contribution to the total AOD closely mirrors the distribution of BB smoke, as
456 anticipated. The contribution of BC to the total AOD is generally small, ranging between 5-10%
457 in BB regions, except for central South Africa where it reaches 10-15%. Despite the higher ratio
458 of BB smoke AOD to total AOD in CAMSRA, the ratio of BC to total AOD over East Asia and
459 South Asia is smaller in CAMSRA compared to MERRA-2 and JRAero, suggesting that BC
460 emissions from anthropogenic sources maybe lower in CAMSRA (also Fig. 2). Finally, the
461 contributions of FM and CM AOD to the total AOD are also depicted in Figure 3. It is consistent

462 among the RAs that FM is the dominant contributor over most land regions except for regions
463 where dust is dominant, such as North Africa, the Arabian Peninsula, the Middle East, and the
464 Gobi. In all the RAs, CM is the dominant contributor over oceanic regions, except for regions
465 influenced by continental BB smoke and pollution outflow. The contribution of CM in CAMSRA
466 is generally smaller in tropical to mid-latitude oceans compared to other RAs, due to its higher
467 contribution from BB smoke. It is also noted that CM is dominant over FM in the Antarctic in
468 NAAPS-RA, while FM is dominant in the Antarctic in the other three RAs, though total AOD is
469 very small (annual and seasonal means < 0.04 from MRC) and hard to validate due to lack of
470 observational data.



471

472 Figure 3. Ratio of speciated AODs, FM and CM AODs to total AOD from the MRC and the
 473 individual RAs based on the 2011-2019 annual average.

474 Table 4 provides a summary of global-average total AOD and speciated AODs, as well as the
 475 contributions of speciated AOD to total AOD for all the RAs. Overall, the annual and global mean
 476 total AODs are similar, hovering around 0.14 for most RAs. All land and ocean mean AODs are
 477 within 0.006 of the MRC with the exception of CAMSRA over ocean, which is higher than the
 478 MRC by +0.024.

479 Speciated AODs, especially smoke AOD and OM/OC AOD display greater divergence among the
 480 RAs. Smoke and OM AODs from CAMSRA are 2-3 times higher than those from the other RAs.
 481 Smoke AOD contributes to 41% of total AOD in CAMSRA, while ranging from 16%-22% in
 482 other RAs. Moreover, the standard deviation of smoke and OM AODs with respect to the 12
 483 months is also higher in CAMSRA than in other RAs. The contribution of dust AOD to total AOD
 484 varies from 13% to 28% for all the RAs, with NAAPS dust AOD being the highest among the RAs
 485 and about 2 times that of CAMSRA, which has the lowest dust AOD among the RAs. The
 486 contribution of sulfate/ABF AOD to total AOD ranges from 23% to 34%, with the highest
 487 contribution observed in JRAero, even larger than the ABF AOD contribution in NAAPS-RA. Sea
 488 salt AOD contributes 25% to 35% to total AOD in the RAs with JRAero being the highest. BC
 489 AOD, on the other hand, contributes only 3% to 4% of total AOD across the RAs. The FM's
 490 contribution to the overall AOD varies across different datasets. In MERRA-2, NAAPS-RA, and
 491 JRAero, FM accounts for 44% to 51% of the total AOD. However, in CAMSRA, its contribution
 492 is notably higher at 63%, primarily due to its significant contribution from OM. Conversely, CM's
 493 contribution to total AOD is consistent across the three RAs, ranging from 49% to 56%. In contrast,
 494 CM's contribution is lower, at 37%, in CAMSRA.

495 Table 4. Global area-weighted mean modal (total, FM, CM) and speciated AOD and standard
 496 deviation of monthly AOD based on 2011-2019 data. Percentage numbers in the brackets are
 497 contributions of speciated AOD to total AOD. Global mean total AODs over land and water are
 498 shown in the last two rows.

	global mean AOD					AOD standard deviation w.r.t. 12 months				
	CAMSRA	MERRA2	NAAPSRA	JRAero	MRC	CAMSRA	MERRA2	NAAPSRA	JRAero	MRC
total	0.151	0.137	0.134	0.134	0.139	0.018	0.010	0.011	0.012	0.013
dust	0.019 (13%)	0.029 (21%)	0.037 (28%)	0.021 (16%)	0.026 (19%)	0.008	0.009	0.009	0.009	0.008
sea salt	0.037 (25%)	0.041 (30%)	0.038 (28%)	0.045 (34%)	0.040 (29%)	0.001	0.001	0.003	0.002	0.001
sulfate/ABF	0.034 (23%)	0.037 (27%)	0.037 (28%)	0.046 (34%)	0.039 (28%)	0.002	0.001	0.001	0.002	0.001
smoke	0.062 (41%)	0.030 (22%)	0.022 (16%)	0.022 (16%)	0.034 (24%)	0.009	0.007	0.007	0.007	0.007
BC x 10	0.061 (4%)	0.059 (4%)	-	0.044 (3%)	0.054 (4%)	0.013	0.009	-	0.008	0.009
OC/OM	0.056 (37%)	0.024 (18%)	-	0.018 (13%)	0.033 (24%)	0.007	0.006	-	0.006	0.006
FM	0.096 (63%)	0.067 (49%)	0.059 (44%)	0.068 (51%)	0.073 (53%)					
CM	0.056 (37%)	0.070 (51%)	0.075 (56%)	0.066 (49%)	0.066 (47%)					
land total	0.180	0.174	0.175	0.176	0.176					
water total	0.136	0.118	0.112	0.111	0.112					

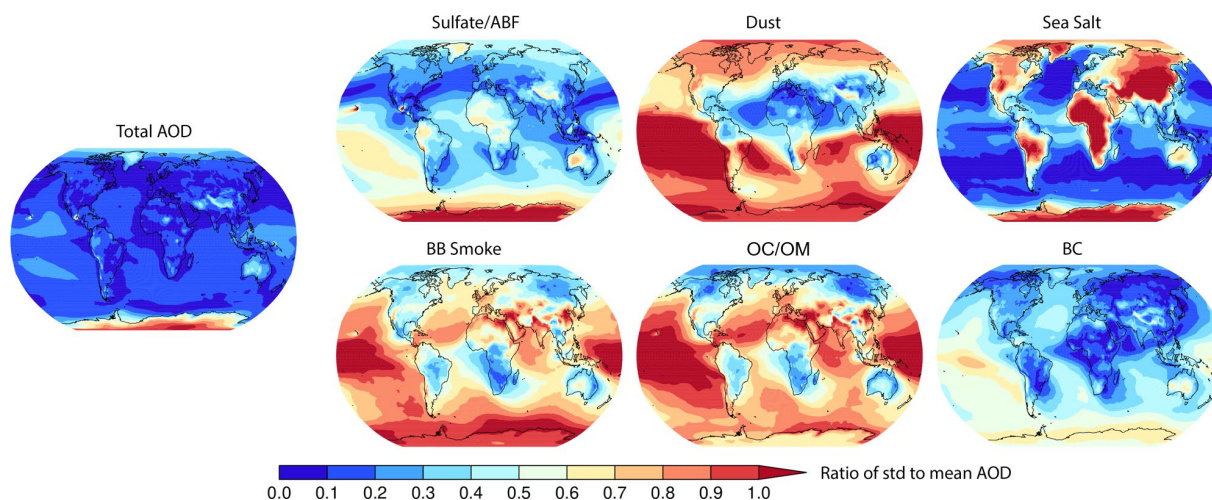
500 3.2 Geographical divergence of speciated AOD among the four RAs

501 The divergence of the global-average total and speciated AODs is already documented in Table 4.
 502 Figure 4 provides the geographical distribution of the relative spread of speciated annual mean
 503 AODs from the RAs to their means. Spread, in this context, is defined as the ratio of the standard
 504 deviation of the RAs AODs to their mean. It is noteworthy that the relative spread of total AOD
 505 from the four RAs is generally small, except for polar regions and specific hotspots where known
 506 issues exist. For instance, biases in CAMSRA AOD have been identified over Hawaii and
 507 Mexico's volcanic outgassing regions. In polar regions, there are limited satellite observations to
 508 constrain model fields, resulting in a larger spread, which is consistent with the findings of Xian

509 et al. (2022) on AODs from CAMSRA, MERRA-2 and NAAPS-RA over the Arctic. Similarly,
 510 over high terrains with snow and ice covers, such as the Himalayas and the Andes, and over desert
 511 regions, such as the Australian deserts, and the Bodele Depression region in the Sahara, both
 512 retrievals and models face challenges, leading to a larger spread. Moreover, over the Maritime
 513 Continent, where high cloud coverage poses challenges to remote sensing retrievals for both AOD
 514 and BB smoke emissions, the spread is also relatively large.

515 The aforementioned characteristics are also evident in the spread of speciated AODs. However,
 516 the spreads of the speciated AODs among the RAs are much larger compared to the total AOD,
 517 particularly in regions that are remote from aerosol sources. This suggests that the efficiency of
 518 removal processes during long-range transport may differ. This is also relevant to the fact that data
 519 assimilation constrains the total AOD, but speciated AOD remains unconstrained. Moreover, the
 520 disparities in definitions of species, such as sulfate/ABF, BB smoke, OC/OM, as discussed in
 521 Section 2.5, can also influence the spread of these FM species. The relative spread of speciated
 522 AODs being much larger than that of total AOD, is broadly consistent with the AeroCom results,
 523 where global climate models (without data assimilation) were intercompared in terms of aerosol
 524 optical properties and life cycles (Kinne et al., 2006; Textor et al., 2006; Glib et al., 2021).

525



526

527 Figure 4. Spread of total and speciated climatological annual-mean AOD among the four RAs.
 528 Spread here is defined as the ratio of the standard deviation of the RA AODs to their mean.

529 3.3. Evaluation with AERONET AOD

530 This section presents evaluation of the monthly performance of the four RAs plus the MRC at the
 531 AERONET sites on regional and global scales. Both skill and consistency of the different RAs and
 532 consensus are evaluated.

533 3.3.1 Bias, RMSE, and correlation between the RAs and AERONET

534
 535 The regional and global mean modal AOD bias, RMSE, and coefficient of determination for the
 536 four RAs and the MRC are shown as bar graphs on global maps in Figures 5, 6 and 7. Regarding

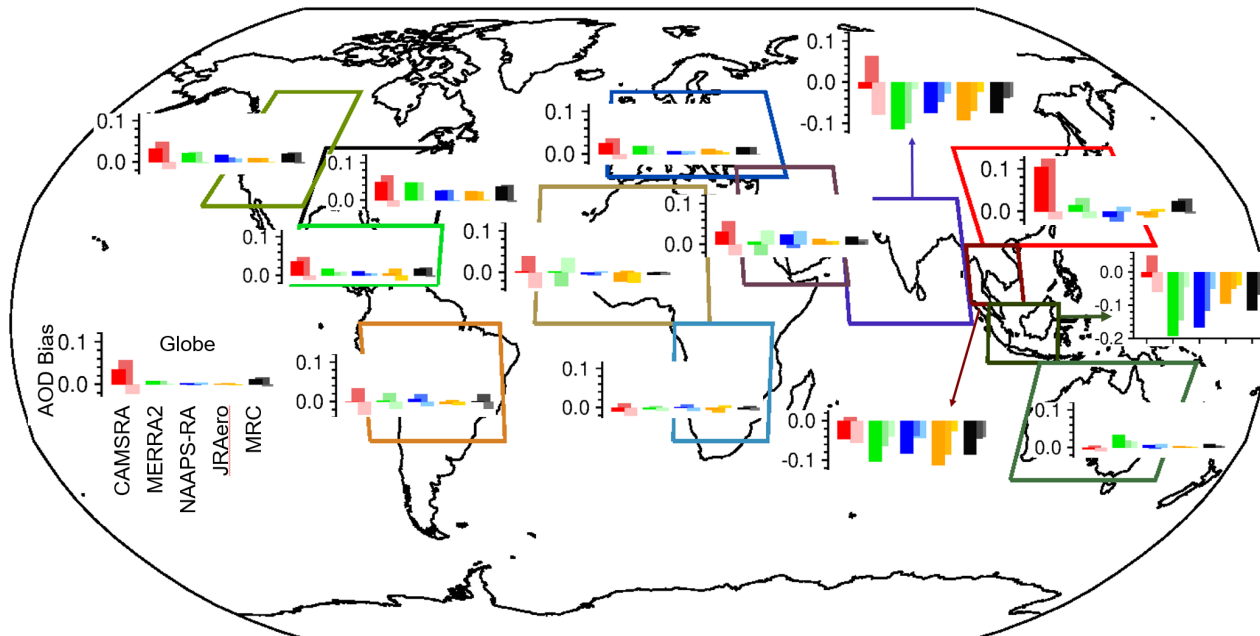
537 regional bias, all the RAs except for CAMSRA, have large negative biases (on the order of -0.1)
538 in total AOD over Southeast Asia, South Asia, and the Maritime continent (Figure 5). The much
539 smaller negative bias in total AOD over these regions in CAMSRA is a result of the cancelation
540 of a positive bias in FM, possibly due to high biased OM/smoke AOD, and a negative bias in CM.
541 The large negative biases over these regions in the other RAs are mainly attributed to large negative
542 biases in FM AOD in general. It is also noted that CAMSRA is biased relatively high in total AOD
543 due to high FM bias over East Asia. Over other regions and the globe, all the RAs have relatively
544 small biases and in general slight positive biases, with CAMSRA having the largest positive bias,
545 due mainly to relatively high OM/smoke AOD. The cancellation effect of positive FM bias and
546 negative CM bias in CAMSRA are also visible.

547
548 Total AOD RMSEs are relatively high over all Asian regions and North Africa compared to other
549 regions for all the RAs (Figure 6). The contribution of FM to total AOD RMSE is larger than that
550 from CM globally, except over dust-influenced region, including North Africa and, for most
551 models, Southwest Asia and Central America. The correlations of total AOD between the RAs and
552 AERONET data are mostly reasonable for all the regions (Figure 7). Some relatively low-
553 performance regions (total AOD r^2 less than 0.60 for at least one RA) include South Asia,
554 Southwest Asia, Australia, Europe, and East Asia. The relatively low correlations over Australia
555 and Europe are due to the low climatological mean and variance. While the other low-performance
556 regions are all mixed pollution and dust environment that is challenging for all RAs. Some
557 relatively high-performance regions (total AOD r^2 greater than 0.85 for at least two RA members)
558 include Central America, Peninsula Southeast Asia, and Maritime Continent. Total and CM AOD
559 r^2 are high over Central America, because it is a receptor region for African dust, and RAs perform
560 well in general during long-range transport over ocean where data assimilation is very effective in
561 correcting model AOD fields. Total and FM AOD r^2 are high over Peninsula Southeast Asia, and
562 Maritime Continent, suggesting the RAs can capture the large interannual variabilities of the
563 regional dominant aerosol species, BB smoke, associated with the impact of ENSO on fire
564 activities in the regions (e.g., Reid et al., 2012; Xian, et al., 2013). Overall, the MRC exhibits
565 superior r^2 compared to individual RAs for modal AODs regionally and globally.

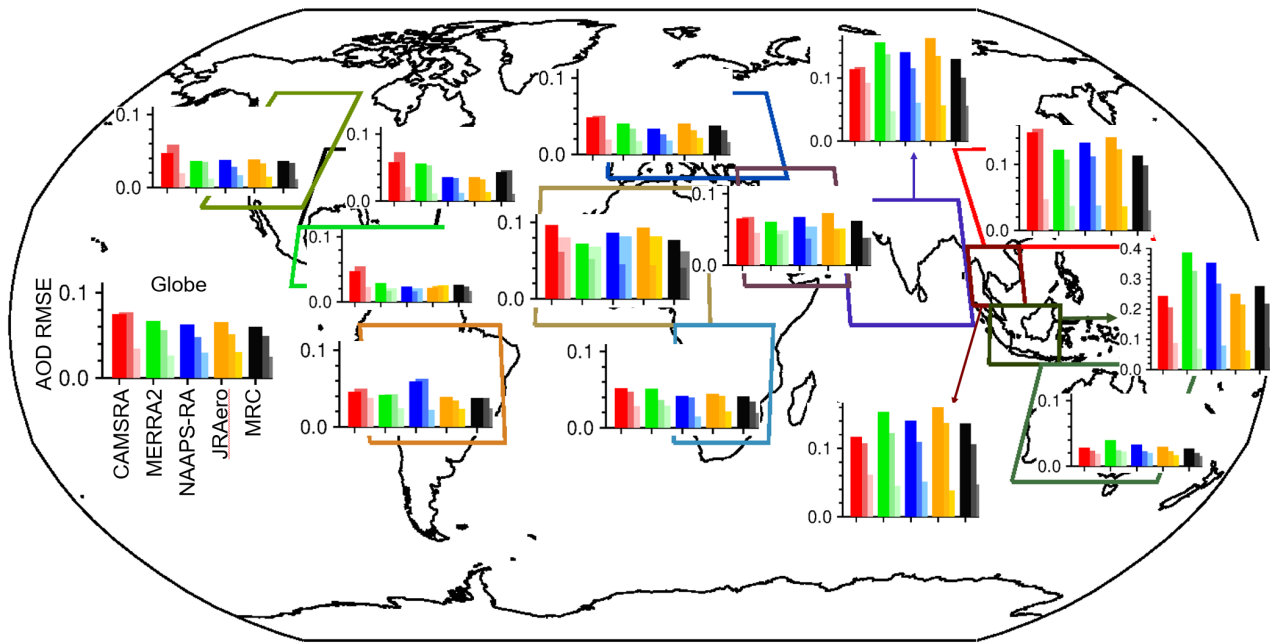
566
567 For remote marine sites, including Ascension Island in the mid-basin of south Atlantic, Ragged
568 Point in the western Tropical Atlantic, Mauna Loa in Hawaii, MCO-Hanimaadhoo in the north
569 Indian Ocean, and REUNION_DENIS in the south Indian Ocean, the RAs exhibit similar
570 performance at these sites as they do over the upwind land or coastal regions (Fig. S1). An
571 exception is Mauna Loa. Mauna Loa is situated at an elevation of 3.4 km, well above the marine
572 boundary layer and remote from continental sources. At this location, all the RAs exhibit a
573 significant positive bias. One possible explanation for this bias is the topographic effect, as the
574 coarse spatial resolutions of the models may not be able to resolve the site's high elevation or its
575 sharp elevation gradient compared to the surroundings. Additionally, uncertainties in the removal
576 processes during long-range transport may also be contributing to the high bias. It is also worth
577 noting that all the RAs do especially well at the Ragged Point site, with total AOD r^2 close to or
578 higher than 0.92. This site is a receptor site of African dust in the Western Tropical Atlantic. This
579 suggests that the RAs capture the long range-transport of dust from Africa quite well. This is
580 related to the fact that data assimilation systems have more chance to correct the model fields with
581 observations in the long-range transport over the ocean.

582

583 When considering the contribution of dust and sea salt aerosols to FM AOD in CAMSRA,
 584 MERRA-2 and JRAero, the verification statistics (bias, RMSE and r^2) for the total AOD of these
 585 RAs remain unchanged as expected (Fig. S2, S3, S4). However, there is a noticeable shift in the
 586 positive bias of FM AOD (and negative bias of CM AOD) for these RAs, particularly in regions
 587 influenced by dust, such as North Africa, the Arabian Peninsula, East Asia, Central America, South
 588 Asia, and Europe. Specifically, the positive bias in FM AOD becomes more pronounced, and the
 589 negative bias in CM AOD becomes more negative in these regions, especially for CAMSRA. It's
 590 worth noting that in MERRA-2, there is a change in sign, where the FM AOD bias switches from
 591 negative to positive in North Africa and the Arabian Peninsula, while the CM AOD bias changes
 592 from positive to negative in these regions. Additionally, the negative FM AOD bias becomes
 593 smaller, however the negative CM AOD bias worsens in South Asia within both MERRA-2 and
 594 JRAero datasets (Fig. S2). In general, when taking into account the contribution of dust and sea
 595 salt aerosols to FM AOD (by default, dust and sea salt AODs are treated as CM AODs in this
 596 study) in CAMSRA, MERRA-2, and JRAero, we observe a worsening of both FM and CM AOD
 597 biases in these three datasets. Similarly, the RMSE for both FM and CM AODs over regions
 598 influenced by dust deteriorates as well (Fig. S3). The r^2 for FM and CM AODs in these regions
 599 also worsens overall, with the exception of an improvement in FM AOD over Central America.
 600 FM sea salt's impact on the verification score is small as the majority of AERONET sites are on
 601 land and FM sea salt only contributes on the order of $\sim 10\%$ to total sea salt AOD in the three RAs.
 602

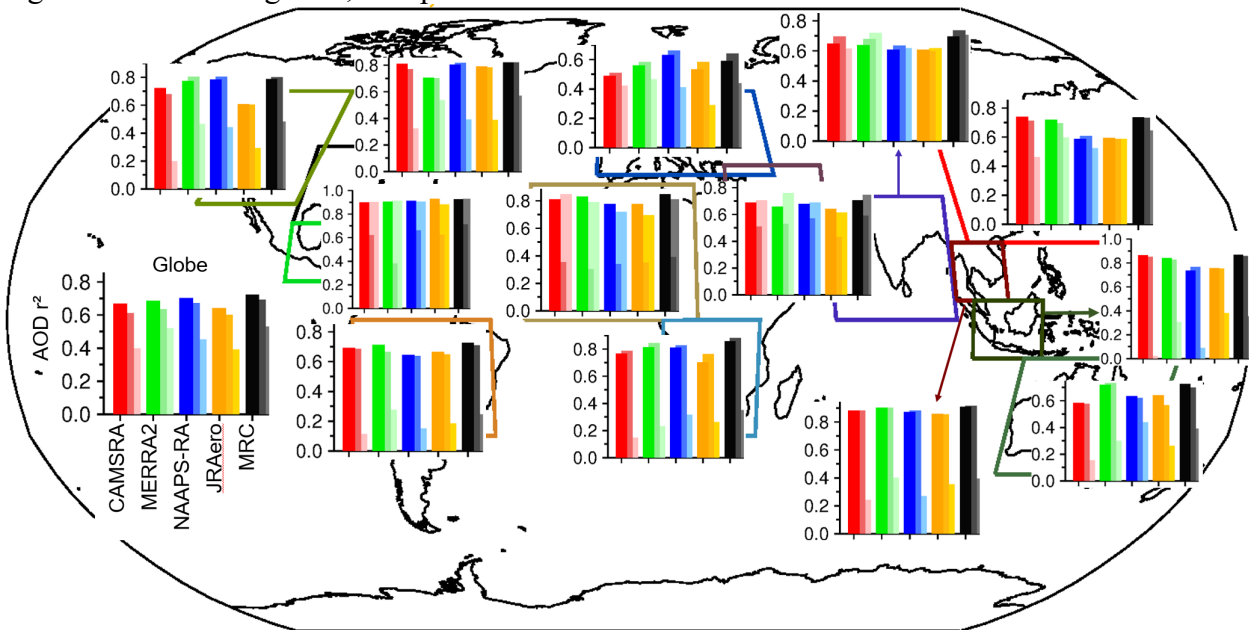


603
 604 Figure 5. Regional total, FM, and CM AOD biases for the four reanalyses and the MRC
 605 compared with AERONET data. Each grouped bars in the same color system present total, FM,
 606 and CM AOD biases from left to right (also dark to light).
 607



608
609
610

Figure 6. Same as Figure 5, except for AOD RMSE.



611
612
613
614

Figure 7. Same as Figure 5, except for the AOD coefficient of determination (r^2).

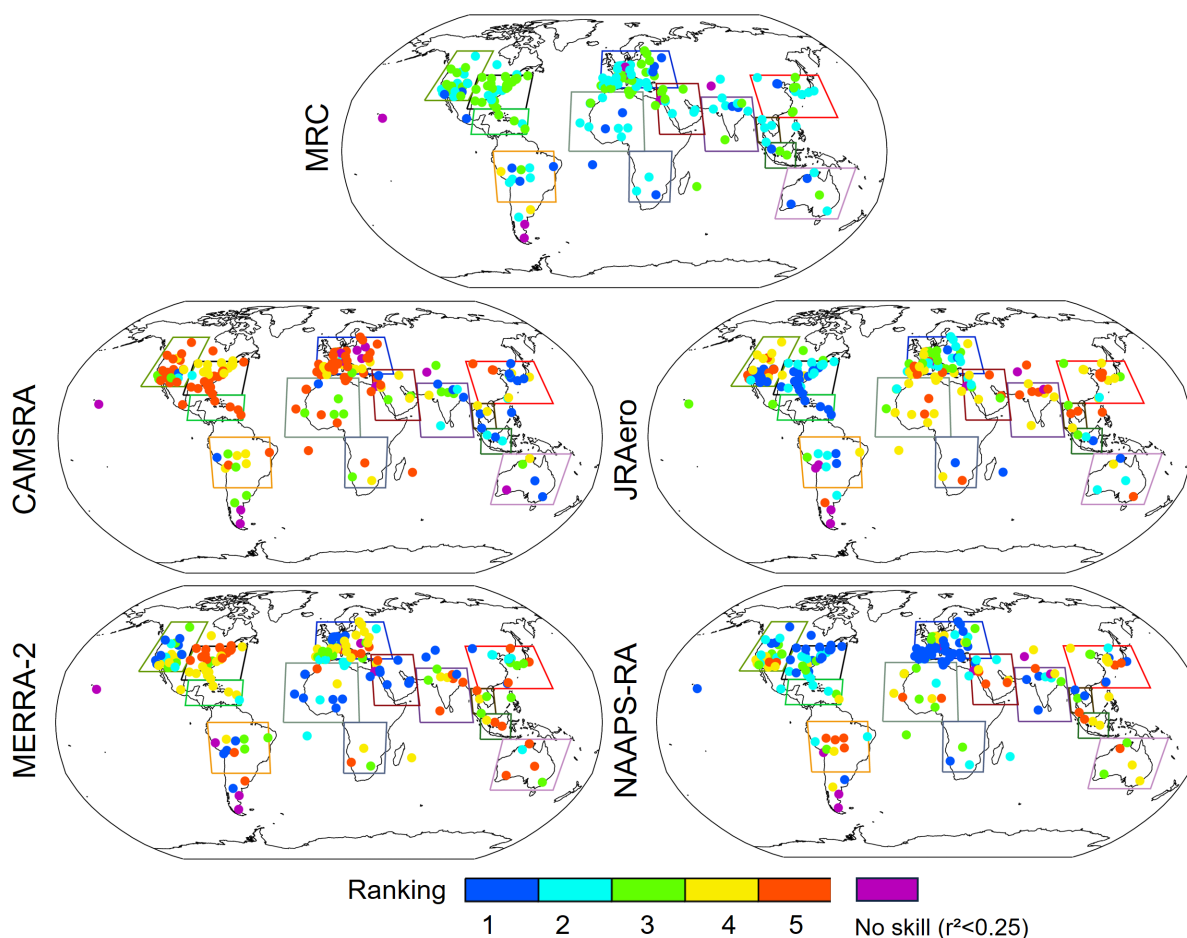
3.3.2 Rankings of the RAs with respect to validation statistics

615 To expand the validation result from regional averages to individual sites, including remote sites
616 that are not included in the regional analysis, rankings of the RAs in terms of RMSE of monthly
617 total AOD at all the AERONET sites are displayed in Figure 8. It shows that there are cases in that
618 individual RA ranks first over some regions. For example, CAMSRA ranks relatively better than
619 others in South and Southeast Asia, MERRA2 ranks better over North Africa and Arabia
620 Peninsula, NAAPS-RA ranks better over North America and Europe while JRAero performs
621

622 relatively better over Southern North America and the Caribbean. Individual RA has mixed results
 623 for sites in other regions. AOD RMSE of the MRC is not always the lowest for a given site, but it
 624 is relatively low and stable over the globe. This is consistent with the regional RMSE result (Figure
 625 6). The consensus wins because of its averaging of independent models. This is consistent with
 626 our findings with the ICAP models (Sessions et al., 2015; Xian et al., 2019).

627
 628 Challenging sites for these RAs are found as marked by the magenta color in Figure 8. These sites
 629 exhibit an r^2 value of less than 0.25, and are associated with relatively large AOD bias and/or
 630 RMSE. Often, when a challenge occurs, it is a common challenge to all models, and no specific
 631 model is much better than the others. Some of the causes for the challenges include lack or large
 632 uncertainty in local emissions (e.g. Modena in Northern Italy, Mainz in Germany, Cario_EMA in
 633 Egypt, Trelew and CEILAP-RG sites in Argentina), and/or topographic effects that are not
 634 resolved in these RAs due mostly to coarse model spatial resolutions (e.g., Mauna_Loa), and sites
 635 that are impacted by mixed pollution and dust (Dushanbe in Tajikistan).

636

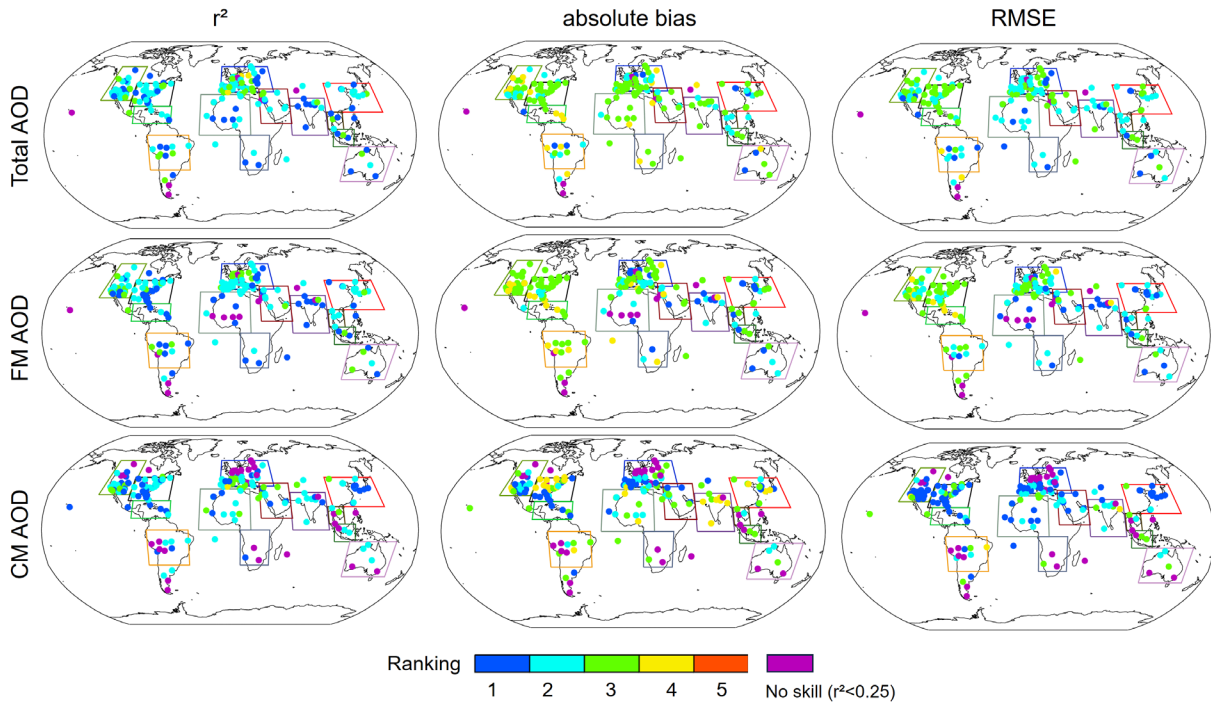


637
 638 Figure 8: Ranking of aerosol RAs in terms of RMSE of monthly total AOD at 550nm over all the
 639 AERONET sites. Rectangles are used to delineate regions for regional validation, as depicted in
 640 Figures 5, 6, 7. A lower RMSE indicates better performance, with a ranking of 1 being the most

641 desirable. AERONET sites with a coefficient of determination (r^2) less than 0.25 are marked in
 642 magenta, indicating a lack of skill from the model.

643

644 Ranking analyses were also conducted on the RMSEs of FM and CM AODs, absolute bias, and r^2
 645 of modal AODs. Figure 9 presents the MRC rankings for all these comparison statistics. In line
 646 with the MRC ranking for the total AOD's RMSE, the MRC rankings for other metrics are
 647 predominantly ranked first or second, except for the absolute biases, where MRC rankings are
 648 often ranked third over North America, South Americas, and Europe for total and FM AODs. For
 649 these modes and over these regions, all the RAs have positive biases relative to AERONET. When
 650 the biases are in the same sign (positive or negative), it is mathematically natural for MRC to rank
 651 in the middle. For CM and FM AODs, there are more sites with $r^2 < 0.25$ compared to the total
 652 AOD. These sites mostly have small values of CM or FM AODs, and reside in regions of opposite-
 653 mode dominance, such as FM in Saharan region, CM in northern Europe and N. America. From
 654 another perspective, the MRC ranking with respect to correlations is superior to RMSE and then
 655 absolute bias. That is, the MRC better captures aerosol variance than the individual models, but is
 656 nevertheless subject to overall model biases. The MRC ranking for CM AOD is slightly superior
 657 to that of total AOD and then FM AOD. While the MRC ranking is not consistently at the top for
 658 a given site or region, it is relatively high and stable, ranking first for the global average. No
 659 individual RAs could compete with the MRC in that sense.



660
 661 Figure 9. Ranking of the MRC among all the RAs in terms of r^2 , absolute bias, and RMSE of the
 662 total, FM, and CM AODs over AERONET sites.

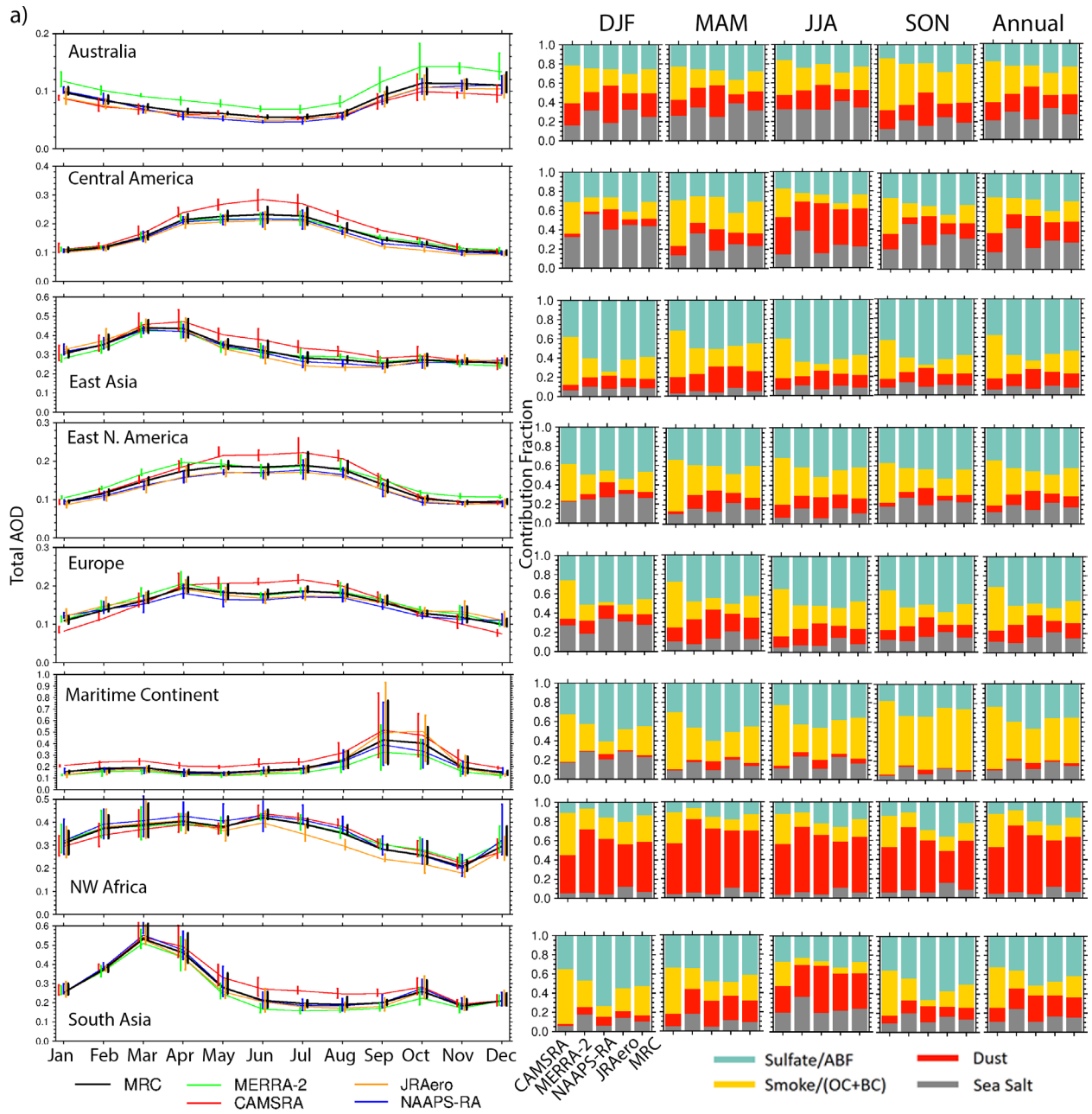
663
 664 3.4 Seasonality of Regional AODs

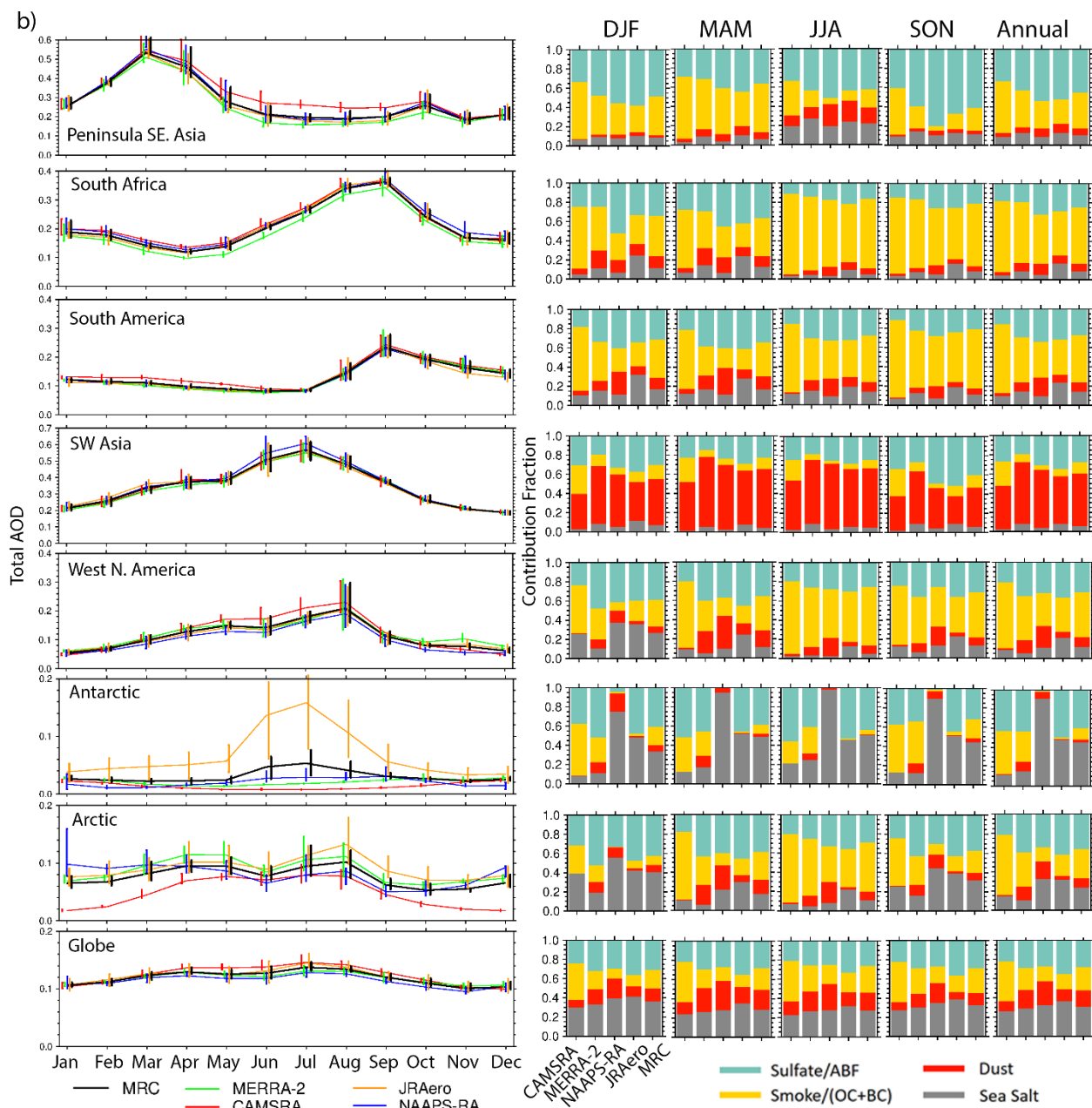
665 In Section 3.1 we depict the spatial distribution of total AODs from all the RAs across the four
 666 seasons. In this section, we provide monthly time series of AOD and AOD interannual variabilities
 667 for 16 regions (Fig. 10), along with the contributions of speciated AOD to the total AOD for these
 668 regions for four seasons and the annual-mean. All the RAs exhibit a similar seasonality and

669 interannual variability of total AOD for all regions, except for the Antarctic and Arctic, particularly
670 during their winter seasons. This disparity arises from the absence of passive satellite AOD data
671 during polar winter, which limits the effect of data assimilation on model AOD (see Xian et al.,
672 2022 for the Arctic region). Even during polar summer, AOD retrievals are often unavailable due
673 to high reflectance from surface ice/snow. The total AOD in JRAero exhibits exceptionally high
674 levels, primarily attributed to elevated sea salt and sulfate AODs (Fig. S5). This anomaly stems
675 from the MASINGAR model used to produce JRAero, which tended to underestimate the removal
676 of aerosols via cumulus convection. Consequently, this led to an overestimation of aerosol
677 concentrations in the polar regions and the upper atmosphere. The underestimation of the removal
678 process has been resolved in the current MASINGAR model and the overestimation of AOD over
679 the polar regions will be improved with the JRAero version upgrade. Nevertheless, the polar
680 regions demonstrate the most significant divergence among the RAs in the seasonal cycle and
681 speciation of AOD.

682
683 The regions that are dominated by BB-smoke, including South Africa, South America, Maritime
684 Continent, Peninsula SE Asia, and western North America, exhibit consistent peak seasons of total
685 AOD with their respective burning seasons. The Maritime Continent and Peninsula SE Asia
686 experience extremely large interannual variations of peak monthly AOD, owing to a strong
687 positive correlation between burning activities and El Nino cycles (e.g., Reid et al., 2012; Xian et
688 al., 2013). The contributions of sulfate/ABF AOD induced by pollution are dominant in East Asia
689 and South Asia, while other aerosol species also make a significant contribution to the total AOD.
690 In Europe and East N. America, sulfate/ABF is also the dominant species; however, the monthly
691 total AOD values are much smaller. All the RAs capture the dominance of dust species in
692 summertime over SW Asia and NW Africa. The relatively high AOD in springtime in NW Africa
693 is partially due to BB in Sahel. In Australia, the peak AOD in Oct-Dec is associated with BB
694 smoke. In Central America, the relatively high AOD in the springtime results from BB smoke.
695 Although quite diverse in AOD magnitude, all RAs tend to have a summertime total AOD peak
696 attributed to dust. For the global average, sea salt AOD has a significant contribution to the total
697 AOD as the area of the ocean overwhelms the area of land. Monthly time series of the speciated
698 AODs for all the regions are available in Fig. S5. Overall, the seasonality and interannual
699 variability of total AOD for most regions is very similar among the RAs. Moreover, all RAs have
700 the same dominant species for most regions, but the contributions from different species can be
701 quite different in these RAs. This is a result of the fact that total AOD is constrained within these
702 RAs through data assimilation, while speciated AODs are not. Aerosol speciation and the
703 contribution of each species to the total AOD are determined by the construction of the aerosol
704 forecast models, which are very independent in these RAs.

705
706
707
708





710
 711 Figure 10. Climatological seasonal cycle of regional mean total AOD (left), and the contribution
 712 fraction of speciated AOD to the total AOD for the corresponding regions and seasons from the
 713 four RAs and the MRC (right). In the seasonal cycle plots, bars denote the interquartile range of
 714 monthly-mean AOD, illustrating interannual variabilities for the period 2011-2019.

715
 716 3.5 Urban versus Rural areas
 717 To evaluate the RAs for urban versus rural areas, three paired sites were selected. Beijing
 718 (China), Yonsei University (South Korea) and Kanpur (India) represent urban areas, while their
 719 corresponding rural areas are represented by the Xiang He, Anmyon and Gandhi College sites
 720 among the available AERONET sites. Fig. 11 shows the monthly time series of modal AODs
 721 from the RAs and the MRC, along with their validation statistics against AERONET data. The
 722 dominant aerosol mode is FM at all these sites, due mostly to pollution. These sites are also

723 subject to the influence of dust storms in springtime, which contributes to CM AOD. The modal
724 AODs from the four RAs and the MRC generally follow these of AERONET seasonally. The
725 spread among the RAs is relatively large for the Chinese and Indian sites. The spread is relative
726 small for the Korean sites, with the spread being slightly less for the rural site Anmyon than for
727 its corresponding urban site Yonsei University. Regarding bias, RMSE, and r^2 , there is no
728 significant difference between the urban and the corresponding rural sites for each RA and the
729 MRC, despite that r^2 of total AOD tending to be higher for the rural sites than the urban sites.
730 The r^2 of FM AOD also tends to be higher than that of the CM. The RAs and the MRC also
731 capture the decreasing AOD trend in the latter half of the 2011-2019 time period for the Chinese
732 and Korean sites. A more detailed trend analysis will be provided in a companion paper. For the
733 ranking of all RAs in terms of bias, RMSE and r^2 , each individual RA has a few first rankings.
734 MERRA-2 is especially better compared to other RAs at CM/dust AOD for the Indian sites. But
735 in terms of the number of ranking first, the MRC is the winner for all the sites (at least having 5
736 out of 9 statistical variables ranking first for each site).

737

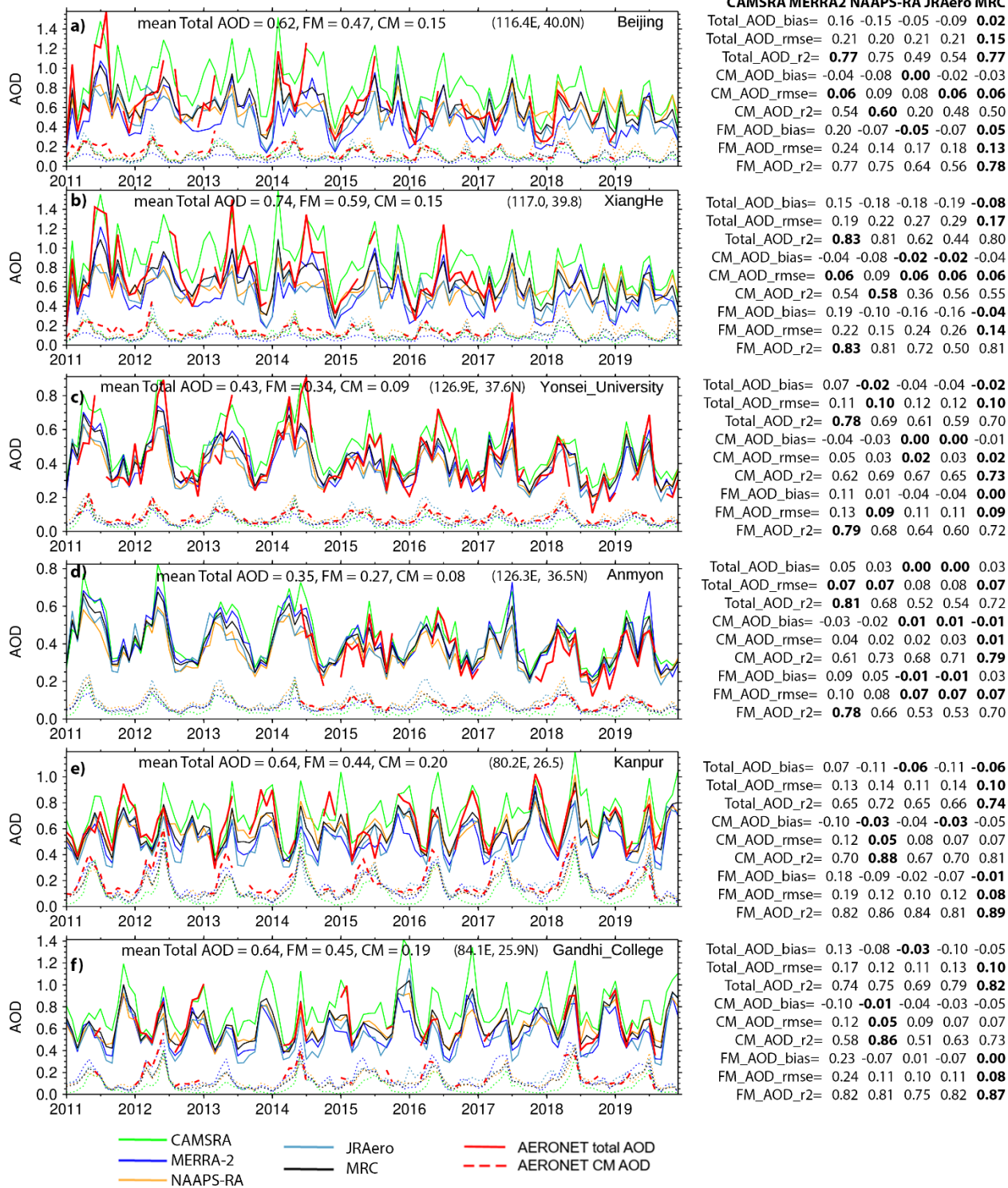


Figure 11. Evaluation of total, FM, and CM monthly AODs from the RAs at urban versus rural AERONET sites. Sites a), c) and e) represent urban locations in China, Korea and India respectively, while sites b), d) and f) denote their corresponding rural sites. Mean Total, FM, and CM AODs from AERONET data are presented in the upper panels of the time series plots for each site. The right column displays verification statistics for the four RAs and the MRC,

745 including bias, RMSE and r^2 . Values in bold indicate the lowest bias or RMSE, or the highest r^2 ,
746 signifying the best ranking among all the RAs.

747
748

749 **4. Conclusions**

750 This study compares the monthly average total, and speciated aerosol optical depths (AODs) from
751 four different aerosol reanalyses (RAs). These include the Copernicus Atmosphere Monitoring
752 Service ReAnalysis (CAMSRA) developed by Copernicus/ECMWF; the Japanese Reanalysis for
753 Aerosol (JRAero) developed at the Japan Meteorological Agency (JMA); the Modern-Era
754 Retrospective Analysis for Research and Applications, version 2 (MERRA-2) developed by
755 NASA; and the Navy Aerosol Analysis and Prediction System reanalysis (NAAPS-RA) version
756 1, developed by the U.S. Naval Research Laboratory. The consensus of the four RAs is also
757 developed for intercomparison. The AODs from these RAs are evaluated with AEROSol Robotic
758 NETwork (AERONET) and the MODIS Dark Target/Deep Blue retrievals (Levy et al., 2013;
759 Sayer et al. (2014)) using data from 2011-2019. The following are the conclusions drawn from this
760 study:

761 1) Global distribution and magnitude of total AOD demonstrate a high level of similarity
762 among all four RAs. The spread of total AOD among the RAs is small over most regions.
763 Exceptions, where the RAs diverge in total AOD are polar regions and areas affected by
764 specific factors that include volcanic outgassing, high terrain, and certain desert regions.

765 2) The relative spread of speciated AODs is considerably larger than that of total AOD.
766 CAMSRA consistently yields higher values for biomass burning (BB) smoke or Organic
767 Matter (OM) AOD in comparison to other RAs. Meanwhile, NAAPS-RA exhibits
768 generally higher dust AOD values. JRAero has comparatively high biased inland sea salt
769 AOD. The divergence of speciated AODs in regions remote from aerosol sources is large,
770 implying different efficiencies in removal during long-range transport. This phenomenon
771 results from the fact that data assimilation in these RAs constrains total AOD but not
772 speciated AOD.

773 3) The seasonality and interannual variability of total AOD in the 16 regions under study,
774 with the exception of the Antarctic and Arctic, demonstrate a high degree of similarity
775 across the various RAs and align with the observations. While the dominant species of
776 aerosols are consistent across most regions in all RAs, the relative contributions from
777 individual species can vary significantly.

778 4) The accuracy of the RAs, as measured by RMSE, bias, and correlation of the total, fine-
779 mode (FM) and coarse-mode (CM) AODs (i.e. modal AODs), has been verified with
780 AERONET. It is evident that each RA exhibits its own unique regional strengths.
781 Specifically, CAMSRA performs better in South and Southeast Asia, MERRA-2 excels in
782 African and Arabian Peninsula dust regions, NAAPS-RA shows relatively better
783 performance over Europe and East CONUS, and JRAero performs relatively better over
784 southern North America and the Caribbean. Common challenges to all the RAs often
785 include lack or large uncertainty in local emissions, and/or topographic effects, as well as

786 situations where both FM and CM states are mixed. There is no significant difference in
787 RAs' performance for urban versus rural areas, despite that rural areas tend to have slightly
788 higher AOD correlations with observations. RAs show the worst performance in areas
789 impacted by mixed FM and CM aerosols, such as South Asia and East Asia, and areas that
790 experience substantial interannual variability in AOD, for instance, Southeast Asia, and the
791 Maritime Continent. The polar regions present a challenge due to limited observations.

792 5) The Multi-Reanalysis-Consensus (MRC), an ensemble mean of the four RAs, is not
793 consistently the best performer in terms of RMSE, bias and correlation of modal AODs for
794 a given site or region. However, the MRC generally performs relatively well and remains
795 stable, ranking first or second regionally and first globally among all the RAs, especially
796 for correlation and RMSE. The MRC ranking with respect to correlations is superior to
797 RMSE and then absolute bias. The MRC ranking for CM AOD is slightly superior to that
798 of total AOD and then FM AOD. The MRC method gains an advantage due to its ability
799 to average independent models.

800 The findings presented in this study offer a comprehensive overview of the current state-of-the-art
801 aerosol RAs in the context of monthly AOD. The strengths and weaknesses of individual RAs and
802 their collective implications will provide valuable information for diverse potential users.
803 Compared to intercomparisons of satellite AOD products, which have shown a typical bias of
804 15%-25% (which regionally can reach $\pm 50\%$) and AOD divergence of 10% over ocean to 100%
805 over certain land areas amongst 14 satellite products in Schutgens et al., 2020, and the
806 intercomparisons of different MODIS products shown in Fig. 1, the biases and divergence of
807 AODs from the four RAs are moderate. The MRC product, which is currently a simple ensemble
808 mean of the four RAs, could be potentially improved with regionally-weighted member
809 contributions according to the strengths of the RAs or with aerosol scenario/species-weighted
810 member contributions.

811 The results of the intercomparison highlight areas for improvement in the next generation of
812 aerosol RAs. These improvements may include tuning of emission sources and sinks, finer
813 spatiotemporal resolutions, incorporation of additional aerosol species, such as nitrate aerosols and
814 dust with different mineralogy, separation of BC and OC from BB emissions in some RAs, and
815 application and enhancement of BB plume rise models. Moreover, some centers are planning to
816 incorporate new observational data, such as OMI Aerosol Index to constrain the amount of
817 absorptive aerosols, which has the potential to enhance simulations of BB smoke and dust aerosols
818 (Zhang et al., 2021; Sorenson et al, 2023). Vertical profiles of aerosol backscatter measured by
819 CALIOP and future space-borne lidars may also be incorporated into RAs to help constrain aerosol
820 vertical distribution. Anticipated advancements in emission inventories, retrieval algorithms,
821 space-borne sensors, upcoming satellite missions, and improvements in meteorological and
822 aerosol modelling are expected to drive progress in aerosol RA.

823 **Appendix A: Abbreviations:**

824 ABF: Anthropogenic and Biogenic Fine aerosols

825 AERONET: Aerosol Robotic Network

826 AOD: Aerosol Optical Depth

827 AVHRR: Advanced Very High Resolution Radiometer

828 BB: Biomass Burning
829 BC: Black Carbon
830 CALIOP: Cloud-Aerosol Lidar with Orthogonal Polarization (CALIOP)
831 CAMSRA: Copernicus Atmosphere Monitoring System Reanalysis
832 CM: Coarse Mode
833 FLAMBE: Fire Locating and Modeling of Burning Emissions
834 FM: Fine Mode
835 ICAP: International Cooperative for Aerosol Predictions
836 JRAero: the Japanese Reanalysis for Aerosol
837 MASINGAR: Model of Aerosol Species IN the Global AtmospheRe
838 MISR: Multi-angle Imaging SpectroRadiometer
839 MME: Multi-Model-Ensemble
840 MODIS: Moderate Resolution Imaging Spectroradiometer
841 MODIS-DT: MODIS Dark Target
842 MODIS-DB: MODIS Deep Blue
843 MODIS-DA: MODIS data assimilation quality data.
844 MRC: Multi-reanalysis-consensus
845 NAAPS-RA v1: Naval Aerosol Analysis and Prediction System-Reanalysis version 1.
846 MERRA-2 :Modern-Era Retrospective Analysis for Research and Applications version 2
847 OM: Organic Matter
848 OC: Organic Carbon
849 OMI: Ozone Monitoring Instrument (OMI)
850 PMAp: Polar Multi-Sensor Aerosol product
851 QFED: Quick Fire Emissions Dataset
852 RA: ReAnalysis
853 RMSE: Root Mean Square Error
854 SDA: Spectral Deconvolution Method

855 **Appendix B: Definition of terminologies**

856 Root Mean Square Error (RMSE):

857
$$\text{RMSE} = \sqrt{\frac{1}{n} \sum_{i=1}^n (\tau_{model} - \tau_{obs})_i^2}$$
 where τ represents monthly AOD, and n is the total number

858 (i.e. month) of observational or model data.

859 Bias: $\tau_{model} - \tau_{obs}$

860 Mean error: $\frac{1}{n} \sum_{i=1}^n (\tau_{model} - \tau_{obs})_i$

861 Mean absolute error: $\frac{1}{n} \sum_{i=1}^n |\tau_{model} - \tau_{obs}|_i$

862 Coefficient of determination: $r^2 = \frac{(\sum_{i=1}^n (x_i - \bar{x})(y_i - \bar{y}))^2}{\sum_{i=1}^n (x_i - \bar{x})(y_i - \bar{y}) \sum_{i=1}^n (x_i - \bar{x})(y_i - \bar{y})}$

863 where \bar{x} and \bar{y} are the mean values of variable x and y .

864 Multi-Reanalysis-Consensus (MRC): $\frac{1}{m} \sum_{i=1}^m x_i$ where m is the total number of the individual
865 reanalysis, which is 4 for this study.

866 Spread among the RAs is defined as the standard deviation of all the individual models, ie.,

867 $\sigma = \sqrt{\frac{1}{m} \sum_{i=1}^m (x_i - \bar{x})^2}$ where x_i is individual reanalysis, and \bar{x} is the MRC.

868 **Data Availability**

869 All the data supporting the findings of this manuscript can be accessed via the provided links or
870 by requesting them using the contact information provided within those links.

871 AERONET Version 3 Level 2 data: <http://aeronet.gsfc.nasa.gov>

872 MODIS data-assimilation-quality AOD:

873 <https://modaps.modaps.eosdis.nasa.gov/services/about/products/c61-nrt/MCDAODHD.html>

874 CAMSRA AOD: <https://www.ecmwf.int/en/research/climate-reanalysis/cams-reanalysis>

875 JRAero product: <https://www.riam.kyushu-u.ac.jp/taikai/JRAero/>

876 MERRA-2 AOD:

877 [https://disc.gsfc.nasa.gov/datasets/M2TMNXAER_V5.12.4/summary?keywords=%22MERRA-
878 2%22](https://disc.gsfc.nasa.gov/datasets/M2TMNXAER_V5.12.4/summary?keywords=%22MERRA-2%22)

879 NAAPS-RA AOD: [https://usgodae.org/cgi-](https://usgodae.org/cgi-bin/datalist.pl?dset=nrl_naaps_reanalysis&summary=Go)

880 [bin/datalist.pl?dset=nrl_naaps_reanalysis&summary=Go](https://usgodae.org/cgi-bin/datalist.pl?dset=nrl_naaps_reanalysis&summary=Go)

881 [MRC AOD: https://nrlgodae1.nrlmry.navy.mil/cgi-](https://nrlgodae1.nrlmry.navy.mil/cgi-bin/datalist.pl?dset=nrl_mre4_post&summary=Go)

882 [bin/datalist.pl?dset=nrl_mre4_post&summary=Go](https://nrlgodae1.nrlmry.navy.mil/cgi-bin/datalist.pl?dset=nrl_mre4_post&summary=Go)

883

884 **Supplement**

885

886 **Author contributions**

887 PX and JSR designed the study. PX performed the data analysis and wrote the paper with
888 contributions from MA, PRC, KY, TFE, EJH, and JZ on data descriptions and information
889 collection. All authors contributed to the discussion of the results and revising the paper.

890 **Competing interests**

891 The contact author has declared that none of the authors has any competing interests.

892 **Acknowledgments**

893 The authors acknowledge financial supports from the Office of Naval Research Code 322. Partial
894 support comes from NASA's Interdisciplinary Science (IDS) program (grant no.
895 80NSSC20K1260). We also thank the NASA AERONET and MODIS teams for the AOD data
896 used in the study. We extend our gratitude to NASA GMAO, ECMWF, JMA, U.S. ONR and NRL
897 for providing access to the aerosol reanalysis products.

898 **References**

- 899 Atwood, S. A., Reid, J. S., Kreidenweis, S. M., Blake, D. R., Jonsson, H. H., Lagrosas, N. D.,
900 Xian, P., Reid, E. A., Sessions, W. R., and Simpas, J. B.: Size-resolved aerosol and cloud
901 condensation nuclei (CCN) properties in the remote marine South China Sea – Part 1:
902 Observations and source classification, *Atmos. Chem. Phys.*, 17, 1105–1123,
903 <https://doi.org/10.5194/acp-17-1105-2017>, 2017.
- 904 Buchard, V., Silva, A. M. da, Colarco, P. R., Darmenov, A., Randles, C. A., Govindaraju, R.,
905 Torres, O., Campbell, J., and Spurr, R. (2015) Using the OMI aerosol index and absorption
906 aerosol optical depth to evaluate the NASA MERRA Aerosol Reanalysis, *Atmos Chem Phys*, 15,
907 5743–5760, <https://doi.org/10.5194/acp-15-5743-2015>.
- 908
- 909 Buchard, V., Randles, C. A., Silva, A. M. da, Darmenov, A., Colarco, P. R., Govindaraju, R.,
910 Ferrare, R., Hair, J., Beyersdorf, A. J., Ziemba, L. D., and Yu, H. (2017) The MERRA-2 Aerosol
911 Reanalysis, 1980 Onward. Part II: Evaluation and Case Studies, *J Climate*,
912 <https://doi.org/10.1175/jcli-d-16-0613.1>.
- 913
- 914 Colarco, P. R., Kahn, R. A., Remer, L. A., and Levy, R. C. : Impact of satellite viewing-swath
915 width on global and regional aerosol optical thickness statistics and trends. *Atmospheric*
916 *Measurement Techniques*, 7, 2313–2335, 2014.
- 917 Cui, C.; Liu, Y.; Chen, L.; Liang, S.; Shan, M.; Zhao, J.; Liu, Y.; Yu, S.; Sun, Y.; Mao, J.;
918 Zhang, H.; Gao, S.; Zhenxing Ma, Z (2022) Assessing public health and economic loss
919 associated with black carbon exposure using monitoring and MERRA-2 data, *Environmental*
920 *Pollution*. 313, 120190, ISSN 0269-7491, doi: <https://doi.org/10.1016/j.envpol.2022.120190>.
- 921 Dee, D. P., and A. M. da Silva (1999) Maximum-likelihood estimation of forecast and
922 observation error covariance parameters. Part I: Methodology. *Mon. Wea. Rev.*, 127, 1811–
923 1834, doi:10.1175/1520-0493(1999)127,1822:MLEOFA.2.0.CO;2.
- 924
- 925 Dee, D., L. Rukhovets, R. Todling, A. M. da Silva, and J. W. Lawson (2001) An adaptive buddy
926 check for observational quality control. *Quart. J. Roy. Meteor. Soc.*, 127, 2451–2471,
927 doi:10.1002/qj.49712757714.
- 928
- 929 Diehl, T., A. Heil, M. Chin, X. Pan, D. Streets, M. Schultz, and S. Kinne (2012) Anthropogenic,
930 biomass burning, and volcanic emissions of black carbon, organic carbon, and SO₂ from 1980 to

931 2010 for hindcast model experiments. *Atmos. Chem. Phys. Discuss.*, 12, 24 895–24 954,
932 doi:10.5194/acpd-12-24895-2012.
933

934 Eck, T.F., Holben, B.N., Reid, J.S., Dubovik, O., Smirnov, A., O’Neill, N.T., Slutsker, I., Kinne,
935 S., 1999. Wavelength dependence of the optical depth of biomass burning, urban, and desert dust
936 aerosols. *J. Geophys. Res.* 104 (D24), 31,333–31,349.

937 Eck, T. F., Holben, B. N., Reid, J. S., Xian, P., Giles, D. M., Sinyuk, A., et al.
938 (2018). Observations of the interaction and transport of fine mode aerosols with cloud and/or
939 fog in Northeast Asia from Aerosol Robotic Network and satellite remote sensing. *Journal of*
940 *Geophysical Research: Atmospheres*, 123, 5560– 5587. <https://doi.org/10.1029/2018JD028313>

941 Edwards, E.-L., Reid, J. S., Xian, P., Burton, S. P., Cook, A. L., Crosbie, E. C., Fenn, M. A.,
942 Ferrare, R. A., Freeman, S. W., Hair, J. W., Harper, D. B., Hostetler, C. A., Robinson, C. E.,
943 Scarino, A. J., Shook, M. A., Sokolowsky, G. A., van den Heever, S. C., Winstead, E. L.,
944 Woods, S., Ziemba, L. D., and Sorooshian, A.: Assessment of NAAPS-RA performance in
945 Maritime Southeast Asia during CAMP²Ex, *Atmos. Chem. Phys.*, 22, 12961–12983,
946 <https://doi.org/10.5194/acp-22-12961-2022>, 2022.
947

948 Flemming, J., Benedetti, A., Inness, A., Engelen, R. J., Jones, L., Huijnen, V., Remy, S.,
949 Parrington, M., Suttie, M., Bozzo, A., Peuch, V.-H., Akritidis, D., and Katragkou, E.: The
950 CAMS interim Reanalysis of Carbon Monoxide, Ozone and Aerosol for 2003–2015, *Atmos.*
951 *Chem. Phys.*, 17, 1945–1983, <https://doi.org/10.5194/acp-17-1945-2017>, 2017.
952

953 Gelaro, R., McCarty, W., Suarez, M. J., Todling, R., Molod, A., Takacs, L., Randles, C. A.,
954 Darmenov, A., Bosilovich, M. G., Reichle, R., Wargan, K., Coy, L., Cullather, R., Draper, C.,
955 Akella, S., Buchard, V., Conaty, A., Silva, A. M. da, Gu, W., Kim, G.-K., Koster, R., Lucchesi,
956 R., Merkova, D., Nielsen, J. E., Partyka, G., Pawson, S., Putman, W., Rienecker, M., Schubert,
957 S. D., Sienkiewicz, M., and Zhao, B.: The Modern-Era Retrospective Analysis for Research and
958 Applications, Version 2 (MERRA-2), *J Climate*, 30, 5419–5454, [https://doi.org/10.1175/jcli-d-](https://doi.org/10.1175/jcli-d-16-0758.1)
959 [16-0758.1](https://doi.org/10.1175/jcli-d-16-0758.1), 2017.

960

961 Giles, D. M., Sinyuk, A., Sorokin, M. G., Schafer, J. S., Smirnov, A., Slutsker, I., Eck, T. F.,
962 Holben, B. N., Lewis, J. R., Campbell, J. R., Welton, E. J., Korkin, S. V., and Lyapustin, A. I.:
963 Advancements in the Aerosol Robotic Network (AERONET) Version 3 database – automated
964 near-real-time quality control algorithm with improved cloud screening for Sun photometer
965 aerosol optical depth (AOD) measurements, *Atmos. Meas. Tech.*, 12, 169–
966 209, <https://doi.org/10.5194/amt-12-169-2019>, 2019.
967

968 Ginoux, Paul, M Chin, I Tegen, J M Prospero, B Holben, O Dubovik, and Shian-Jiann Lin:
969 Sources and distributions of dust aerosols simulated with the GOCART model. *J. Geophys. Res.*,
970 106(D17), 20255-20273, 2001.

971 Gliß, J., A. Mortier, M. Schulz, E. Andrews, Y. Balkanski, S.E. Bauer, A.M.K. Benedictow, H.
972 Bian, R. Checa-Garcia, M. Chin, P. Ginoux, J.J. Griesfeller, A. Heckel, Z. Kipling, A. Kirkevåg,

973 H. Kokkola, P. Laj, P. Le Sager, M.T. Lund, C. Lund Myhre, H. Matsui, G. Myhre, D. Neubauer,
974 T. van Noije, P. North, D.J.L. Olivié, L. Sogacheva, T. Takemura, K. Tsigaridis, and S.G. Tsyro,
975 2021: AeroCom phase III multi-model evaluation of the aerosol life cycle and optical properties
976 using ground- and space-based remote sensing as well as surface in situ observations. *Atmos.*
977 *Chem. Phys.*, **21**, no. 1, 87-128, doi:10.5194/acp-21-87-2021.

978 Gong, S. (2003) A parameterization of sea-salt aerosol source function for sub- and super-micron
979 particles, *Global Biogeochem Cy*, 17, 1097, <https://doi.org/10.1029/2003gb002079>.

980 Granier, C., Bessagnet, B., Bond, T., D'Angiola, A., van der Gon, H. D., Frost, G. J., Heil, A.,
981 Kaiser, J. W., Kinne, S., Klimont, Z., Kloster, S., Lamarque, J.-F., Liousse, C., Masui, T.,
982 Meleux, F., Mieville, A., Ohara, T., Raut, J.-C., Riahi, K., Schultz, M. G., Smith, S. J.,
983 Thompson, A., van Aardenne, J., van der Werf, G. R., and van Vuuren, D. P.: Evolution of
984 anthropogenic and biomass burning emissions of air pollutants at global and regional scales
985 during the 1980–2010 period, *Climate Change*, 109, 163–190, 2011.

986 Gumber, A., Reid, J. S., Holz, R. E., Eck, T. F., Hsu, N. C., Levy, R. C., Zhang, J., and Veglio,
987 P.: Assessment of Severe Aerosol Events from NASA MODIS and VIIRS Aerosol Products for
988 Data Assimilation and Climate Continuity, *Atmos. Meas. Tech. Discuss.* [preprint],
989 <https://doi.org/10.5194/amt-2022-290>, in review, 2022

990 Hogan, T.F. and T.E. Rosmond: The description of the Navy Operational Global Atmospheric
991 Prediction System's spectral forecast model. *Mon. Wea. Rev.*, 119, 1786-1815, 1991.

992 Hogan, T. F., Liu, M., Ridout, J. S., Peng, M. S., Whitcomb, T. R., Ruston, B. C., Reynolds, C.
993 A., Eckermann S. D., Moskaitis, J. R., Baker, N. L., McCormack, J. P., Viner, K. C., McLay, J.
994 G., Flatau, M. K., Xu, L., Chen, C., and Chang, S. W.: The Navy Global Environmental Model.
995 *Oceanography*, Special Issue on Navy Operational Models, 27, No. 3. 2014.

996 Holben, B. N., Eck, T. F., Slutsker, I., Tanre, D., Buis, J. P., Setzer, A., Vermote, E., Reagan, J.
997 A., Kaufman, Y. J., Nakajima, T., Lavenu, F., Jankowiak, I., and Smirnov, A.: AERONET – A
998 federated instrument network and data archive for aerosol characterization, *Remote Sens.*
999 *Environ.*, 66, 1–16, 1998.

1000 Hsu, N. C., Jeong, M.-J., Bettenhausen, C., Sayer, A. M., Hansell, R., Seftor, C. S., Huang, J.,
1001 and Tsay, S.-C. (2013), Enhanced Deep Blue aerosol retrieval algorithm: The second
1002 generation, *J. Geophys. Res. Atmos.*, 118, 9296– 9315, doi:[10.1002/jgrd.50712](https://doi.org/10.1002/jgrd.50712).

1003 Hyer, E. J., Reid, J. S., and Zhang, J.: An over-land aerosol optical depth data set for data
1004 assimilation by filtering, correction, and aggregation of MODIS Collection 5 optical depth
1005 retrievals, *Atmos. Meas. Tech.*, 4, 379–408, <https://doi.org/10.5194/amt-4-379-2011>, 2011.

1006 Ignatov, A., & Stowe, L. (2002). Aerosol Retrievals from Individual AVHRR Channels. Part I:
1007 Retrieval Algorithm and Transition from Dave to 6S Radiative Transfer Model, *Journal of the*
1008 *Atmospheric Sciences*, 59(3), 313-334. Doi: [https://doi.org/10.1175/1520-](https://doi.org/10.1175/1520-0469(2002)059<0313:ARFIAC>2.0.CO;2)
1009 [0469\(2002\)059<0313:ARFIAC>2.0.CO;2](https://doi.org/10.1175/1520-0469(2002)059<0313:ARFIAC>2.0.CO;2)

1010 Inness, A., Ades, M., Agustí-Panareda, A., Barré, J., Benedictow, A., Blechschmidt, A.-M.,
1011 Dominguez, J. J., Engelen, R., Eskes, H., Flemming, J., Huijnen, V., Jones, L., Kipling, Z.,
1012 Massart, S., Parrington, M., Peuch, V.-H., Razinger, M., Remy, S., Schulz, M., and Suttie, M.:
1013 The CAMS reanalysis of atmospheric composition, *Atmos. Chem. Phys.*, 19, 3515–3556,
1014 <https://doi.org/10.5194/acp-19-3515-2019>, 2019.

1015 Kahn, R. A., Gaitley, B. J., Garay, M. J., Diner, D. J., Eck, T. F., Smirnov, A., and Holben, B.
1016 N. (2010), Multiangle Imaging SpectroRadiometer global aerosol product assessment by
1017 comparison with the Aerosol Robotic Network, *J. Geophys. Res.*, 115, D23209,
1018 doi:[10.1029/2010JD014601](https://doi.org/10.1029/2010JD014601).

1019 Kaiser, J. W., Heil, A., Andreae, M. O., Benedetti, A., Chubarova, N., Jones, L., Morcrette, J.-J.,
1020 Razinger, M., Schultz, M. G., Suttie, M., and van der Werf, G. R.: Biomass burning emis-
1021 sions estimated with a global fire assimilation system based on observed fire radiative power,
1022 *Biogeosciences*, 9, 527–554, <https://doi.org/10.5194/bg-9-527-2012>, 2012.

1023 Kinne, S., Schulz, M., Textor, C., Guibert, S., Balkanski, Y., Bauer, S. E., Berntsen, T., Berglen,
1024 T. F., Boucher, O., Chin, M., Collins, W., Dentener, F., Diehl, T., Easter, R., Feichter, J.,
1025 Fillmore, D., Ghan, S., Ginoux, P., Gong, S., Grini, A., Hendricks, J., Herzog, M., Horowitz, L.,
1026 Isaksen, I., Iversen, T., Kirkevåg, A., Kloster, S., Koch, D., Kristjansson, J. E., Krol, M., Lauer,
1027 A., Lamarque, J. F., Lesins, G., Liu, X., Lohmann, U., Montanaro, V., Myhre, G., Penner, J.,
1028 Pitari, G., Reddy, S., Seland, O., Stier, P., Takemura, T., and Tie, X.: An AeroCom initial
1029 assessment – optical properties in aerosol component modules of global models, *Atmos. Chem.*
1030 *Phys.*, 6, 1815–1834, <https://doi.org/10.5194/acp-6-1815-2006>, 2006.
1031

1032 Kramer, S. J., Alvarez, C., Barkley, A. E., Colarco, P. R., Custals, L., Delgado, R., Gaston, C.
1033 J., Govindaraju, R., and Zuidema, P.: Apparent dust size discrepancy in aerosol reanalysis in
1034 north African dust after long-range transport, *Atmos. Chem. Phys.*, 20, 10047–10062,
1035 <https://doi.org/10.5194/acp-20-10047-2020>, 2020.
1036

1037 Jaegle, L., Quinn, P. K., Bates, T. S., Alexander, B., and Lin, J.-T., (2011) Global distribution of
1038 sea salt aerosols: new constraints from in situ and remote sensing observations, *Atmos Chem*
1039 *Phys*, 11, 3137–3157, <https://doi.org/10.5194/acp-11-3137-2011>.

1040 Jenwitheesuk, K.; Peansukwech, U.; Jenwitheesuk, K., (2022) Predictive MERRA-2 aerosol
1041 diagnostic model for oral, oropharyngeal and laryngeal cancer caused by air pollution in Thai
1042 population, *Toxicology Reports*, 9, 970-978. Doi: <https://doi.org/10.1016/j.toxrep.2022.04.015>.
1043

1044 Lacima, A., Petetin, H., Soret, A., Bowdalo, D., Jorba, O., Chen, Z., Méndez Turrubiates, R. F.,
1045 Achebak, H., Ballester, J., and Pérez García-Pando, C.: Long-term evaluation of surface air
1046 pollution in CAMSRA and MERRA-2 global reanalyses over Europe (2003–2020), *Geosci.*
1047 *Model Dev. Discuss.* [preprint], <https://doi.org/10.5194/gmd-2022-197>, in review, 2022.
1048

1049 Levy, R. C.; Mattoo, S.; Munchak, L. A.; Remer, L. A.; Sayer, A. M.; Patadia, F.; Hsu, N. C.
1050 The Collection 6 MODIS aerosol products over land and ocean, *Atmos. Meas. Tech.*, 2013, 6,
1051 2989-3034, <https://doi.org/10.5194/amt-6-2989-2013>.
1052

1053 Lynch, P., Reid, J. S., Westphal, D. L., Zhang, J., Hogan, T. F., Hyer, E. J., Curtis, C. A., Hegg,
1054 D. A., Shi, Y., Campbell, J. R., Rubin, J. I., Sessions, W. R., Turk, F. J., and Walker, A. L.: An
1055 11-year global gridded aerosol optical thickness reanalysis (v1.0) for atmospheric and climate
1056 sciences, *Geosci. Model Dev.*, 9, 1489–1522, <https://doi.org/10.5194/gmd-9-1489-2016>, 2016.

1057 McCoy, D. T., F. A.-M. Bender, J. K. C. Mohrmann, D. L. Hartmann, R. Wood, and D. P.
1058 Grosvenor (2017): The global aerosol-cloud first indirect effect estimated using MODIS,
1059 MERRA, and AeroCom, *J. Geophys. Res. Atmos.*, 122, 1779–1796, doi:10.1002/2016JD026141.

1060 Monahan, E. C., Spiel, D. E., and Davidson, K. L.: A model of marine aerosol generation via
1061 whitecaps and wave disruption, in *Oceanic Whitecaps*, edited by: Monahan, E. and Niocaill, G.
1062 M., D. Reidel, Norwell, Mass., 167–174, 1986.

1063 Ningombam, Shantikumar S., Dumka, Umesh Chandra, Mugil, Sivasamy Kalamani, Kuniyal,
1064 Jagdish Chandra, Hooda, Rakesh K., Gautam, Alok Sagar, and Tiwari, Suresh, 2021, "Impacts of
1065 Aerosol Loading in the Hindu Kush Himalayan Region Based on MERRA-2 Reanalysis Data"
1066 *Atmosphere* Vol. 12, No. 10, pp 1290, 2073-4433

1067 Ohno, T., Irie, H., Momoi, M. and da Silva, A.M. : Quantitative evaluation of mixed biomass
1068 burning and anthropogenic aerosols over the Indochina Peninsula using MERRA-2 reanalysis
1069 products validated by sky radiometer and MAX-DOAS observations. *Prog Earth Planet Sci* 9, 61
1070 (2022). <https://doi.org/10.1186/s40645-022-00520-4>

1071
1072 O'Neill, N.T., Eck, T. F., Holben, B. N., Smirnov, A., Dubovik, O. and Royer, A.: Bimodal size
1073 distribution influences on the variation of Angstrom derivatives in spectral and optical depth
1074 space, *J. Geophys. Res.*, 106, 9787-9806, 2001.

1075
1076 O'Neill, N. T., Eck, T. F., Smirnov, A., Holben, B. N., and Thulasiraman, S.: Spectral
1077 discrimination of coarse and fine mode optical depth. *J. Geophys. Res.*, 108, D05212,
1078 doi:10.1029/2002JD002975, 2003.

1079
1080 O'Sullivan, D., Marengo, F., Ryder, C. L., Pradhan, Y., Kipling, Z., Johnson, B., Benedetti, A.,
1081 Brooks, M., McGill, M., Yorks, J., and Selmer, P.: Models transport Saharan dust too low in the
1082 atmosphere: a comparison of the MetUM and CAMS forecasts with observations, *Atmos. Chem.*
1083 *Phys.*, 20, 12955–12982, <https://doi.org/10.5194/acp-20-12955-2020>, 2020.

1084
1085 Popp, T., deLeeuw, G., Bingen, C., Brühl, C., Capelle, V., Chedin, A., Clarisse, L., Dubovik, O.,
1086 Grainger, R., Griesfeller, J., Heckel, A., Kinne, S., Klüser, L., Kosmale, M., Kolmonen, P.,
1087 Lelli, L., Litvinov, P., Mei, L., North, P., Pinnock, S., Povey, A., Robert, C., Schulz, M.,
1088 Sogacheva, L., Stebel, K., Zweers, D. S., Thomas, G., Gijssbert Tilstra, L., Vandenbussche, S.,
1089 Veefkind, P., Vountas, M., and Xue, Y.: Development, production and evaluation of aerosol
1090 climate data records from European satellite observations (Aerosol_cci), *Remote Sensing*, 8,
1091 421, <https://doi.org/10.3390/rs8050421>, 2016.

1092 Randles, C. A., daSilva, A. M., Buchard, V., Colarco, P. R., Darmenov, A., Govindaraju, R., et
1093 al.: The MERRA-2 aerosol reanalysis, 1980 onward. Part I: System description and data
1094 assimilation evaluation. *Journal of Climate*, 30(17), 6823-6850. [https://doi.org/10.1175/JCLI-D-](https://doi.org/10.1175/JCLI-D-16-0609.1)
1095 [16-0609.1](https://doi.org/10.1175/JCLI-D-16-0609.1), 2017.

1096 Reid, J.S., Gumber, A. ; Zhang, J.; Holz, R. E.; Rubin, J. I.; Xian, P.; Smirnov, A.; Eck, T. F.;
1097 O’Neill, N. T.; Levy, R. C.; Reid, E. A.; Colarco, P. R.; Benedetti, A.; and Tanaka, T. (2022) A
1098 Coupled Evaluation of Operational MODIS and Model Aerosol Products for Maritime
1099 Environments Using Sun Photometry: Evaluation of the Fine and Coarse Mode. *Remote Sens*,
1100 14, 2978. <https://doi.org/10.3390/rs14132978>.

1101 Reid, J. S., and Coauthors, 2023: The coupling between tropical meteorology, aerosol lifecycle,
1102 convection, and radiation, during the Cloud, Aerosol and Monsoon Processes Philippines
1103 Experiment (CAMP2Ex). *Bull. Amer. Meteor. Soc.*, E1179-E1205,
1104 <https://doi.org/10.1175/BAMS-D-21-0285.1>

1105 Reid, J. S., Hyer, E. J., Prins, E. M., Westphal, D. L., Zhang, J., Wang, J., Christopher, S. A.,
1106 Curtis, C. A., Schmidt, C. C., Eleuterio, D. P., Richardson, K. A., and Hoffman, J. P.: Global
1107 Monitoring and Forecasting of Biomass-Burning Smoke: Description of and Lessons from the
1108 Fire Locating and Modeling of Burning Emissions (FLAMBE) Program, *IEEE J. Sel. Top.*
1109 *Appl.*, 2, 144–162, JSTARS-2009-00034, 2009.

1110 Reid, J. S., Xian, P., Hyer, E. J., Flatau, M. K., Ramirez, E. M., Turk, F. J., Sampson, C. R.,
1111 Zhang, C., Fukada, E. M., and Maloney, E. D.: Multi-scale meteorological conceptual analysis of
1112 observed active fire hotspot activity and smoke optical depth in the Maritime Continent, *Atmos.*
1113 *Chem. Phys.*, 12, 2117–2147, <https://doi.org/10.5194/acp-12-2117-2012>, 2012.

1114 Reid, J. S., Xian, P., Holben, B. N., Hyer, E. J., Reid, E. A., Salinas, S. V., Zhang, J., Campbell,
1115 J. R., Chew, B. N., Holz, R. E., Kuciauskas, A. P., Lagrosas, N., Posselt, D. J., Sampson, C. R.,
1116 Walker, A. L., Welton, E. J., and Zhang, C.: Aerosol meteorology of the Maritime Continent for
1117 the 2012 7SEAS southwest monsoon intensive study – Part 1: regional-scale phenomena, *Atmos.*
1118 *Chem. Phys.*, 16, 14041–14056, <https://doi.org/10.5194/acp-16-14041-2016>, 2016.

1119 Roychoudhury, C., He, C., Kumar, R., McKinnon, J. M., & Arellano, A. F. Jr. (2022). On the
1120 relevance of aerosols to snow cover variability over High Mountain Asia. *Geophysical Research*
1121 *Letters*, 49, e2022GL099317. <https://doi.org/10.1029/2022GL099317>

1122 Sayer, A.M., Munchak, L.A., Hsu, N.C., Levy, R.C., Bettenhausen, C., Jeong, M.J., 2014.
1123 MODIS Collection 6 aerosol products: comparison between Aqua’s e-Deep Blue, Dark Target,
1124 and “merged” _data sets, and usage recommendations. *J. Geophys. Res. Atmos.* 119 (24), 13–
1125 965.

1126 Schutgens, N., Sayer, A. M., Heckel, A., Hsu, C., Jethva, H., de Leeuw, G., Leonard, P. J. T.,
1127 Levy, R. C., Lipponen, A., Lyapustin, A., North, P., Popp, T., Poulsen, C., Sawyer, V.,
1128 Sogacheva, L., Thomas, G., Torres, O., Wang, Y., Kinne, S., Schulz, M., and Stier, P.: An
1129 AeroCom–AeroSat study: intercomparison of satellite AOD datasets for aerosol model

1130 evaluation, *Atmos. Chem. Phys.*, 20, 12431–12457, <https://doi.org/10.5194/acp-20-12431-2020>,
1131 2020.
1132
1133 Sessions, W. R., Reid, J. S., Benedetti, A., Colarco, P. R., da Silva, A., Lu, S., Sekiyama, T.,
1134 Tanaka, T. Y., Baldasano, J. M., Basart, S., Brooks, M. E., Eck, T. F., Iredell, M., Hansen, J. A.,
1135 Jorba, O. C., Juang, H.-M. H., Lynch, P., Morcrette, J.-J., Moorthi, S., Mulcahy, J., Pradhan, Y.,
1136 Razingerg, M., Sampson, C. B., Wang, J., and Westphal, D. L. (2015) Development towards a
1137 global operational aerosol consensus: basic climatological characteristics of the International
1138 Cooperative for Aerosol Prediction Multi-Model Ensemble (ICAP-MME), *Atmos. Chem. Phys.*,
1139 15, 335-362
1140
1141 Shi, Y., Zhang, J., Reid, J. S., Hyer, E. J., and Hsu, N. C.: Critical evaluation of the MODIS
1142 Deep Blue aerosol optical depth product for data assimilation over North Africa, *Atmos. Meas.*
1143 *Tech.*, 6, 949–969, <https://doi.org/10.5194/amt-6-949-2013>, 2013.
1144
1145 Shi, Y., Zhang, J., Reid, J. S., Holben, B., Hyer, E. J., and Curtis, C.: An analysis of the
1146 collection 5 MODIS over-ocean aerosol optical depth product for its implication in aerosol
1147 assimilation, *Atmos. Chem. Phys.*, 11, 557–565, <https://doi.org/10.5194/acp-11-557-2011>, 2011.
1148
1149 Sorenson, B. T., Zhang, J., Reid, J. S., Xian, P., and Jaker, S. L.: Ozone Monitoring Instrument
1150 (OMI) UV aerosol index data analysis over the Arctic region for future data assimilation and
1151 climate forcing applications, *Atmos. Chem. Phys.*, 23, 7161–7175, [https://doi.org/10.5194/acp-](https://doi.org/10.5194/acp-23-7161-2023)
1152 [23-7161-2023](https://doi.org/10.5194/acp-23-7161-2023), 2023.
1153
1154 Textor, C., Schulz, M., Guibert, S., Kinne, S., Balkanski, Y., Bauer, S., Bernsten, T., Berglen, T.,
1155 Boucher, O., Chin, M., Dentener, F., Diehl, T., Easter, R., Feichter, H., Fillmore, D., Ghan, S.,
1156 Ginoux, P., Gong, S., Grini, A., Hendricks, J., Horowitz, L., Huang, P., Isaksen, I., Iversen, I.,
1157 Kloster, S., Koch, D., Kirkevåg, A., Kristjansson, J. E., Krol, M., Lauer, A., Lamarque, J. F., Liu,
1158 X., Montanaro, V., Myhre, G., Penner, J., Pitari, G., Reddy, S., Seland, Ø., Stier, P., Takemura,
1159 T., and Tie, X.: Analysis and quantification of the diversities of aerosol life cycles within
1160 AeroCom, *Atmos. Chem. Phys.*, 6, 1777–1813, <https://doi.org/10.5194/acp-6-1777-2006>, 2006.
1161
1162 Tong, D. Q., et al., Health and Safety Effects of Airborne Soil Dust in the Americas and Beyond.
1163 *Reviews of Geophysics.* <https://doi.org/10.1029/2021RG000763>
1164
1165 Xian, P., Klotzbach, P. J., Dunion, J. P., Janiga, M. A., Reid, J. S., Colarco, P. R., and Kipling,
1166 Z.: Revisiting the relationship between Atlantic dust and tropical cyclone activity using aerosol
1167 optical depth reanalyses: 2003–2018, *Atmos. Chem. Phys.*, 20, 15357–15378,
1168 <https://doi.org/10.5194/acp-20-15357-2020>, 2020.
1169
1170 Xian, P., Reid J. S., Hyer, E., Sampson, C.R., Rubin, J., Ades M., et. al., Current state of the
1171 global operational aerosol multi-model ensemble: an update from the International Cooperative
1172 for Aerosol Prediction (ICAP), *Quarterly J. of the Royal Met. Soc.*
1173 <https://doi.org/10.1002/qj.3497>, 2019.
1174

- 1175 Xian, P., Reid, J. S., Turk, J. F., Hyer, E. J., and Westphal, D. L.: Impact of models versus
1176 satellite measured tropical precipitation on regional smoke optical thickness in an aerosol
1177 transport model, *Geophys. Res. Lett.*, 36, L16805, doi:10.1029/2009GL038823, 2009.
1178
- 1179 Xian, P. Reid, J. S., Atwood, S. A., Johnson, R. S., Hyer, E. J., Westphal, D. L., Sessions, W.:
1180 Smoke aerosol transport patterns over the Maritime continent, *Atmos. Res.* Vol. 122, 469-485,
1181 <https://doi.org/10.1016/j.atmosres.2012.05.006>
- 1182 Xian, P., Zhang, J., O'Neill, N. T., Toth, T. D., Sorenson, B., Colarco, P. R., Kipling, Z., Hyer, E.
1183 J., Campbell, J. R., Reid, J. S., and Ranjbar, K.: Arctic spring and summertime aerosol optical
1184 depth baseline from long-term observations and model reanalyses – Part 1: Climatology and
1185 trend, *Atmos. Chem. Phys.*, 22, 9915–9947, <https://doi.org/10.5194/acp-22-9915-2022>, 2022.
- 1186 Witek, M. L., P. J. Flatau, P. K. Quinn, and D. L. Westphal: Global sea-salt modeling: Results
1187 and validation against multicampaign shipboard measurements, *J. Geophys. Res.*, 112, 2007.
- 1188 Yumimoto, K., Tanaka, T. Y., Oshima, N., and Maki, T.: JRAero: the Japanese Reanalysis for
1189 Aerosol v1.0, *Geosci. Model Dev.*, 10, 3225–3253, <https://doi.org/10.5194/gmd-10-3225-2017>,
1190 2017.
- 1191 Yukimoto, S., Adachi, Y., Hosaka, M., Sakami, T., Yoshimura, H., Hirabara, M., Tanaka, T. Y.,
1192 Shindo, E., Tsujino, H., Deushi, M., Mizuta, R., Yabu, S., Obata, A., Nakano, H., Koshiro, T.,
1193 Ose, T., and Kitoh, A.: A New Global Climate Model of the Meteorological Research Institute:
1194 MRI-CGCM3 –Model Description and Basic Performance, *J. Meteorol. Soc. Jpn.*, 90A, 23–64,
1195 <https://doi.org/10.2151/jmsj.2012-A02>, 2012.
- 1196 Zhang, J. L., and J. S. Reid: MODIS aerosol product analysis for data assimilation: Assessment
1197 of over-ocean level 2 aerosol optical thickness retrievals. *J. Geophys. Res.-Atmos.*, 111, 2006.
1198
- 1199 Zhang, J. L., and Reid, J. S., Westphal, D. L., Baker, N. L., and Hyer, E. J.: A system for
1200 operational aerosol optical depth data assimilation over global oceans. *J. Geophys. Res.*, 113,
1201 D10208, doi:10.1029/2007JD009065, 2008.
1202
- 1203 Zhang J., Reid, J. S., Alfaro-Contreras, R., Xian P., Has China been exporting less particulate air
1204 pollution over the past decade?, *Geophysical Research Letters*, 10.1002/2017GL072617, 2017.
1205
- 1206 Zhang, J., Spurr, R. J. D., Reid, J. S., Xian, P., Colarco, P. R., Campbell, J. R., Hyer, E. J., and
1207 Baker, N. L.: Development of an Ozone Monitoring Instrument (OMI) aerosol index (AI) data
1208 assimilation scheme for aerosol modeling over bright surfaces – a step toward direct radiance
1209 assimilation in the UV spectrum, *Geosci. Model Dev.*, 14, 27–42, <https://doi.org/10.5194/gmd-14-27-2021>, 2021.
1210
- 1211
- 1212 Zhang, X., and Zhou, Y.: Aerosol direct radiative forcing over China: A 40-year MERRA-2-
1213 based evaluation, *Atmos. Env.*, Vol., 299, <https://doi.org/10.1016/j.atmosenv.2023.119659>